
This manuscript is a preprint and has been submitted for publication in *Journal of Geophysical Research: Solid Earth*. Please note that the manuscript is undergoing peer review and has not been accepted for publication. Subsequent versions of this manuscript may have slightly different content. If accepted, the final version of this manuscript will be available via the Peer-reviewed Publication DOI link on the right-hand side of this webpage. Please feel free to contact the corresponding author; we welcome feedback.

Precursory slow slip and foreshocks on rough faults

Camilla Cattania^{1,2} and Paul Segall¹

¹Department of Geophysics, Stanford University, Stanford, CA

²Now at Department of Earth, Atmospheric, and Planetary Sciences, Massachusetts Institute of
Technology, Cambridge, MA

Key Points:

- Rough fault simulations exhibit simultaneous foreshocks and creep caused by heterogeneity in normal stress
- Stress transfer between foreshocks and creep produces a positive feedback and $1/t$ acceleration prior to the mainshock
- The precursory phase is characterized by migratory seismicity and creep over an extended region

Corresponding author: Camilla Cattania, camcat@mit.edu

13 **Abstract**

14 Foreshocks are not uncommon prior to large earthquakes, but their physical mechanism
15 remains controversial. Two interpretations have been advanced: 1. foreshocks are driven
16 by aseismic nucleation; 2. foreshocks are cascades, with each event triggered by earlier
17 ones. Here we study seismic cycles on faults with fractal roughness at wavelengths ex-
18 ceeding the nucleation length. We perform 2-D quasi-dynamic, elastic simulations of fric-
19 tionally uniform rate-state faults. Roughness leads to a range of slip behavior between
20 system-size ruptures, including widespread creep, localized slow slip, and microseismic-
21 ity. These processes are explained by spatial variations in normal stress (σ) caused by
22 roughness: regions with low σ tend to creep, while high σ regions remain locked until
23 they break seismically. Foreshocks and mainshocks both initiate from the rupture of locked
24 asperities, but mainshocks preferentially start on stronger asperities. The preseismic phase
25 is characterized by feedback between creep and foreshocks: episodic seismic bursts break
26 groups of nearby asperities, causing creep to accelerate, which in turns loads other as-
27 perities leading to further foreshocks. A simple analytical treatment of this mutual stress
28 transfer, confirmed by simulations, predicts slip velocities and seismicity rates increase
29 as $1/t$, where t is the time to the mainshock. The model reproduces the observed mi-
30 gration of foreshocks towards the mainshock hypocenter, foreshock locations consistent
31 with static stress changes, and the $1/t$ acceleration in stacked catalogs. Instead of in-
32 terpreting foreshocks as either driven by coseismic stress changes or by creep, we pro-
33 pose that earthquake nucleation on rough faults is driven by the feedback between the
34 two.

Plain Language Summary

Understanding premonitory seismicity leading up to large earthquakes has been a central problem in seismology for several decades. In spite of constantly improving observational networks and data analysis tools, we are still grappling with the fundamental question: what causes foreshocks? Do they represent a chain of isolated events, or are they driven by slow slip over a large fault area, gradually accelerating before the main-shock? In this study, we tackle this question with numerical simulations of slip on a fault with a realistic (fractal) geometry. This geometrical complexity causes spatial variations in stress: compression or extension occur as irregularities on opposite sides of the fault are pressed closer together or pulled apart. This spatial heterogeneity modulates slip stability across the fault, causing simultaneous occurrence of slow slip and foreshocks. The two processes are linked by a positive feedback, since each increases stresses at the location of the other; under certain conditions, this can culminate in a large earthquake. Our model reproduces a number of observed foreshock characteristics, and offers new insights on the physical mechanism driving them.

1 Introduction

Foreshocks have been observed before many moderate and large earthquakes (Abercrombie & Mori, 1996; Jones & Molnar, 1976; Trugman & Ross, 2019; Ende & Ampuero, 2020), and even though modern seismic networks and analysis techniques have imaged foreshock sequences in unprecedented detail (Ellsworth & Bulut, 2018; Tape et al., 2018), the physical mechanisms driving them remains debated (Gomberg, 2018; Mignan, 2014). One interpretation is that foreshocks represent failures of seismic sources (asperities) driven by an otherwise aseismic nucleation process (Tape et al., 2018; Bouchon et al., 2013, 2011; Sagan et al., 2014; McGuire et al., 2005; Abercrombie & Mori, 1996; Ruiz et al., 2014; A. Kato, Fukuda, Nakagawa, & Obara, 2016). Aseismic acceleration prior to instability is predicted by theory (Ruina, 1983; Dieterich, 1992; Rubin & Ampuero, 2005; Ampuero & Rubin, 2008) and has been observed in laboratory experiments (Dieterich & Kilgore, 1996; McLaskey & Lockner, 2014; McLaskey, 2019) and numerical simulations (e.g. Dieterich, 1992; Lapusta et al., 2000; Lapusta, 2003). On the other hand, foreshocks have been interpreted as a cascade of events triggered by one another, not mediated by an aseismic process (Helmstetter & Sornette, 2003; Hardebeck et al., 2008; Schurr et al., 2014). Recent studies have shown that the relative locations of foreshocks are in fact consistent

67 with static stress triggering (Ellsworth & Bulut, 2018; Yoon et al., 2019), and the lack
68 of detectable aseismic slip preceding most moderate to large earthquakes supports the
69 view of a triggering cascade.

70 The occurrence of foreshocks implies fault heterogeneity: if they are driven aseis-
71 mically, heterogeneity leads to simultaneous occurrence of seismic and slow slip; in the
72 cascade model, it is required to explain why foreshocks remain small, while the main-
73 shock evolves into a large rupture. Previous modeling studies of foreshocks have consid-
74 ered various sources of heterogeneity: velocity weakening asperities in a velocity strength-
75 ening fault (Dublanche, 2018; Yabe & Ide, 2018); spatial variations in nucleation length
76 on a velocity weakening fault caused by heterogeneous state evolution distance (Noda
77 et al., 2013) or effective normal stress (Schaal & Lapusta, 2019). In these studies, aseis-
78 mic slip can take place around the asperity due to either velocity strengthening behav-
79 ior or frictional properties that lead to large nucleation dimensions; however, the pres-
80 ence of asperities with a small nucleation dimension can nevertheless lead to a cascad-
81 ing sequence (Noda et al., 2013).

82 Perhaps the most ubiquitous and best characterized source of heterogeneity is ge-
83 ometrical roughness: faults are fractal surfaces (Power et al., 1987, 1988; Power & Tullis,
84 1991; Sagy et al., 2007; Candela et al., 2009, 2012; Brodsky et al., 2016). Numerical and
85 theoretical studies have shown that fault roughness has a first order effect on rupture
86 nucleation (Tal et al., 2018), as well as propagation and arrest (Fang & Dunham, 2013;
87 Dunham et al., 2011; Heimisson, 2020; Ozawa et al., 2019).

88 Here we focus on the effect of long wavelength roughness (exceeding the nucleation
89 length) on the nucleation phase and precursory seismicity leading up to a mainshock.
90 We perform quasi-dynamic simulations of rough but otherwise uniform velocity-weakening
91 faults embedded in a linear elastic medium. Numerical simulations show that a rich slip
92 behavior ranging from slow slip to seismic ruptures arises as a consequence of normal
93 stress heterogeneity induced by fault roughness, which causes spatial variations in strength
94 and fault stability. Early in the cycle, low normal stress regions start to creep stably while
95 high normal stress regions (from now on referred to as “asperities”) remain locked. The
96 mainshock nucleation phase is characterized by an interplay between accelerating creep
97 and episodic foreshocks: creep loads asperities, until they fail seismically; foreshocks in-
98 crease stress on nearby asperities and creeping areas, causing the latter to accelerate in

99 turn triggering subsequent foreshocks; asperities don't fully relock after failure, gradu-
 100 ally unpinning the fault and increasing the creeping area and velocities. We introduce
 101 a simple analytical model based on these interactions, which predicts acceleration in seis-
 102 micity rate and creep as $1/t$, where t is the time to the mainshock. Simulated sequences
 103 reproduce a number of observations, such as the relative location of foreshocks, their mi-
 104 gration towards the mainshock hypocenter and the power-law acceleration of foreshocks
 105 in stacked catalogs.

106 2 Numerical model

107 We run 2-D plane strain simulations with the quasi-dynamic boundary element code
 108 *FDRA* (Segall & Bradley, 2012). The following equation of motion governs fault slip:

$$\tau_{el}(\mathbf{x}) - \tau_f(\mathbf{x}) = \frac{\mu}{2c_s}v(\mathbf{x}), \quad (1)$$

109 where μ is the shear modulus, τ_f the frictional resistance, and τ_{el} the shear stress due
 110 to remote loading and stress interactions between elements. The stress from each ele-
 111 ment is computed from dislocation solutions (e.g., Segall, 2010), accounting for variable
 112 element orientation. The right hand side is the radiation damping term, which repre-
 113 sents stress change due to radiation of plane S-waves (Rice, 1993), with c_s the shear wave
 114 speed.

115 Frictional resistance evolves according to rate-state friction (Dieterich, 1978):

$$\tau_f(v, \theta) = \sigma \left[f_0 + a \log \frac{v}{v_0} + b \log \frac{\theta v_0}{d_c} \right], \quad (2)$$

116 where, a , b and are constitutive parameters; d_c is the state evolution distance; σ is the
 117 effective normal stress; v^* a reference slip velocity; f_0 the steady-state friction coefficient
 118 at $v = v^*$, and θ is a state-variable. Model parameters are listed in table 1. We em-
 119 ploy the ageing law (Ruina, 1983) for state evolution:

$$\frac{d\theta}{dt} = 1 - \frac{\theta v}{d_c}, \quad (3)$$

120 such that steady-state friction at sliding velocity v is

$$f_{ss}(v) = f_0 + (a - b) \log \frac{v}{v^*}. \quad (4)$$

121 We apply remote loading such that the stress-rate tensor is pure shear:

$$\dot{\sigma}_1 - \dot{\sigma}_3 \equiv \dot{\sigma}_D \quad (5)$$

$$\dot{\sigma}_1 + \dot{\sigma}_3 = 0, \quad (6)$$

122 where $\sigma_{1,3}$ are the principal stresses and σ_D the differential stress. Resolving these on
 123 to the fault yields shear and normal stressing rates:

$$\dot{\tau} = \frac{\dot{\sigma}_D}{2} \sin(2\Psi + 2\theta) \quad (7)$$

$$\dot{\sigma} = \frac{\dot{\sigma}_D}{2} \cos(2\Psi + 2\theta), \quad (8)$$

124 where Ψ is the average fault angle with respect to σ_1 and $\theta(x)$ the local slope. In gen-
 125 eral, both shear and normal stress vary in time; here we take $\Psi = 45^\circ$, so that the spa-
 126 tially averaged effective normal stress is constant and equal to a uniform value $\sigma_0 = 10\text{MPa}$.
 127 In addition to the remote loading, slip on a rough fault also causes normal stress changes,
 128 which in our case dominate the effect of spatially variable loading rate described by equa-
 129 tions (7) and (8). In Appendix A we show how perturbations in normal stress depend
 130 on fault roughness and slip. Normal stresses can locally become tensile and induce open-
 131 ing if a purely elastic response is assumed. In contrast, tensile stresses are reduced or
 132 entirely inhibited in an elasto-plastic medium with a Drucker-Prager yield surface (e.g.
 133 Dunham et al., 2011). We approximate this behavior by setting a minimum value σ_{min}
 134 for normal stress, $\sigma_{min} = 1 \text{ kPa} \ll \sigma_0$. Earthquakes are defined as times when the slip
 135 velocity anywhere on the fault exceeds the threshold velocity $V_{dyn} = 2a\sigma c_s/\mu$ (Rubin
 136 & Ampuero, 2005), here $\sim 4 \text{ cm/s}$.

137 The fault profile is fractal, characterized by power spectral density

$$138 \quad P_h = C_h |k|^{-\beta} \quad (9)$$

139 with $\beta = 2H + 1$, where H is the Hurst exponent. For natural faults this is typically
 140 between 0.4–0.8 (Renard & Candela, 2017); here we set $H = 0.7$. For computational
 141 reasons, we only include wavelengths greater than $L_{min} = 100\text{m}$, close to the nominal
 142 nucleation length defined below, unless otherwise specified.

143 2.1 Model resolution

144 To correctly describe rupture behavior, both the nucleation length and the cohe-
 145 sive zone Λ_0 need to be well resolved (e.g. Lapusta et al., 2000; Perfettini & Ampuero,
 146 2008). Erickson et al. (2020) found that a suite of planar fault models, including *FDRA*,
 147 produced well resolved simulations with $\Lambda_0/\Delta x \geq 3$, with $\Lambda_0 = \mu' d_c/b\sigma$ (Rubin, 2008),
 148 in agreement with previous studies (Day et al., 2005). A resolution of $\Lambda_0/\Delta x \approx 1.7$ pro-

Table 1. Model parameters. L_f is the total fault length and $\dot{\tau}$ the spatially averaged stressing rate. Other parameters are described in the text.

Parameter	Value
a	0.015
b	0.02
d_c	10^{-4}m
f_0	0.6
σ_0	10 MPa
$\dot{\tau}$	0.004 Pa s^{-1}
μ	30GPa
ν	0.25
L_{min}	100 m
L_f	5.2 km
C_h	$0.013 \text{ m}^{2(1-H)}$
H	0.7

149 deduced similar temporal patterns, but slight differences in the frequency-magnitude dis-
150 tribution of simulated events. On a rough fault, normal stresses change with time and
151 can locally be higher than the average, requiring a finer resolution. Moreover, we found
152 that rough fault simulations are less forgiving than may be expected from the results above.
153 For instance, a simulation resolving the nominal cohesive zone size with 4 grid points and
154 a small fraction (10 – 15%) of the fault with $\Lambda_0/\Delta x \approx 1 - 2$ produced abundant mi-
155 croseismicity and no full ruptures, while doubling the number of grid points generated
156 full ruptures. Since earthquakes tend to arrest where σ is high and the cohesive zone is
157 small, a few under-resolved regions can determine the event size statistics. Here we spec-
158 ify a uniform resolution with nominal $\Lambda_0/\Delta x \approx 8$, and for the foreshock sequence dis-
159 cussed through most of the paper $\Lambda_0/\Delta x > 2$ everywhere. We tested a few individual
160 foreshocks and verified that their rupture length does not change when doubling the res-
161 olution.

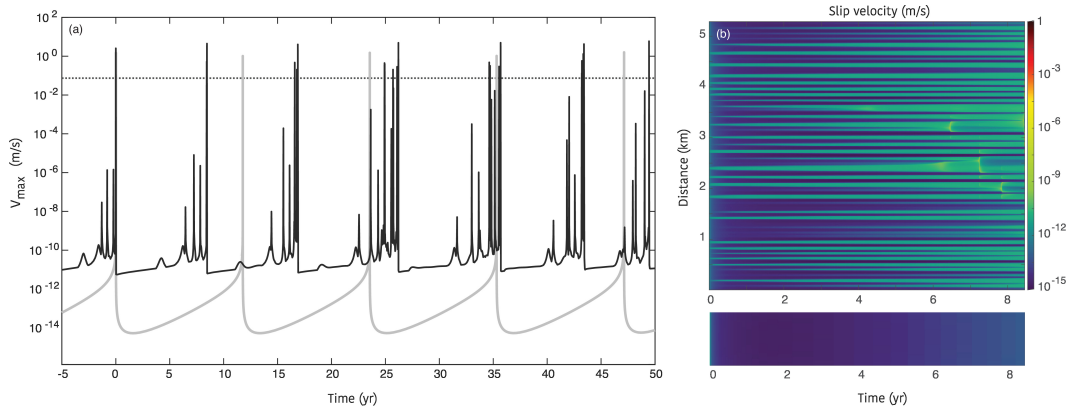


Figure 1. (a) Maximum slip velocity over multiple cycles on a rough (black) and comparable planar (grey) fault. The dotted line is the threshold velocity used to define earthquakes. (b) Slip velocity across the entire fault during one cycle showing alternating creeping and locked patches. The lower panel shows the slip velocity on a planar fault during the same time period (only a small region is shown, since velocity is effectively uniform).

162 3 Summary of simulation results

163 The first order effect of fault roughness during the interseismic phase is a decrease
 164 in fault locking: as seen in Fig. 1(a), and previously noted by Tal et al. (2018), the max-
 165 imum slip velocity on the fault during the interseismic period is several orders of mag-
 166 nitude larger for a rough fault than for its planar counterpart. Fig. 1(b) shows that this
 167 is due to patches of higher velocity between locked patches. For simplicity, in the remain-
 168 der of the paper we refer to these slowly slipping regions as “creeping”, even though their
 169 slip velocity (estimated in section 4) can be several orders of magnitude lower than typ-
 170 ically measurable fault creep.

171 During most of the interseismic phase the average slip velocity slowly increases, as
 172 creeping patches widen; this process is entirely aseismic, even though brief slow slip episodes
 173 with velocities up to about $10^{-6} - 10^{-5}$ m/s occur as creep fronts coalesce and break
 174 asperities (Fig. 1, 6–8 years into the cycle). Only in the final part of the cycle do as-
 175 perities rupture in seismic events while creep rates increase (Fig. 2). During the accel-
 176 eration leading up to the mainshock slip velocity on the fault does not increase gradu-
 177 ally but in abrupt steps, associated with bursts of microseismicity. This pattern repeats
 178 at increasingly short temporal scales as the background slip velocity increases.

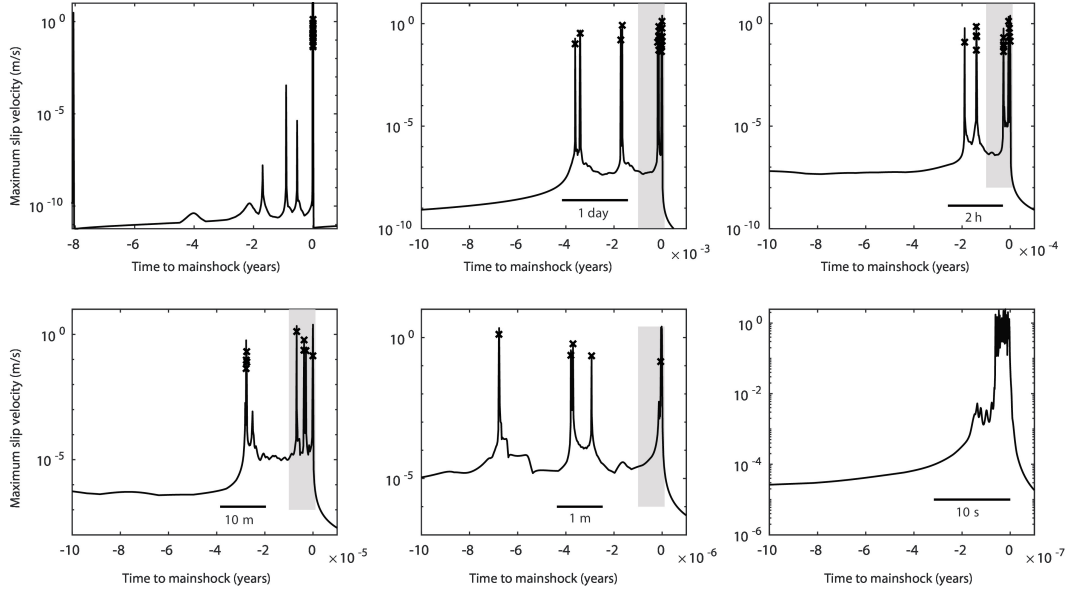


Figure 2. Average slip velocity on the fault leading up to the mainshock, showing a similar pattern across multiple temporal scales. Earthquakes are marked with crosses, and each grey box indicates the extent of the next panel.

179 Foreshocks only occur once sufficient slip has accumulated on the fault, and the first
 180 few sequences consist of events spanning the entire domain (system-size ruptures). This
 181 is due to an increase in the amplitude of normal stress perturbations with total slip, quan-
 182 tified in Appendix A: microseismicity starts when the root-mean-square normal stress
 183 perturbation $\Delta\sigma_{rms}$ is of the order of the background normal stress σ_0 . In the rest of
 184 the paper we will focus on one of the first sequences with foreshocks ($\Delta\sigma_{rms}/\sigma_0 = 1.1$),
 185 since later sequences, with more net slip, may not be well resolved (as discussed in sec-
 186 tion 2). Other sequences are qualitatively similar (Supplementary Figure 1).

187 **4 Relationship between fault roughness and interseismic locking**

188 Previous studies have shown that slip on a rough surface leads to perturbations in
 189 normal stress (Chester & Chester, 2000; Sagy & Lyakhovskiy, 2019; Dunham et al., 2011).
 190 In Appendix A we summarize these findings and derive a simple expression for normal
 191 stress perturbations as a function of cumulative slip and fault topography. Normal stress
 192 perturbations on a fractal fault with uniform slip S have a Gaussian distribution; for a

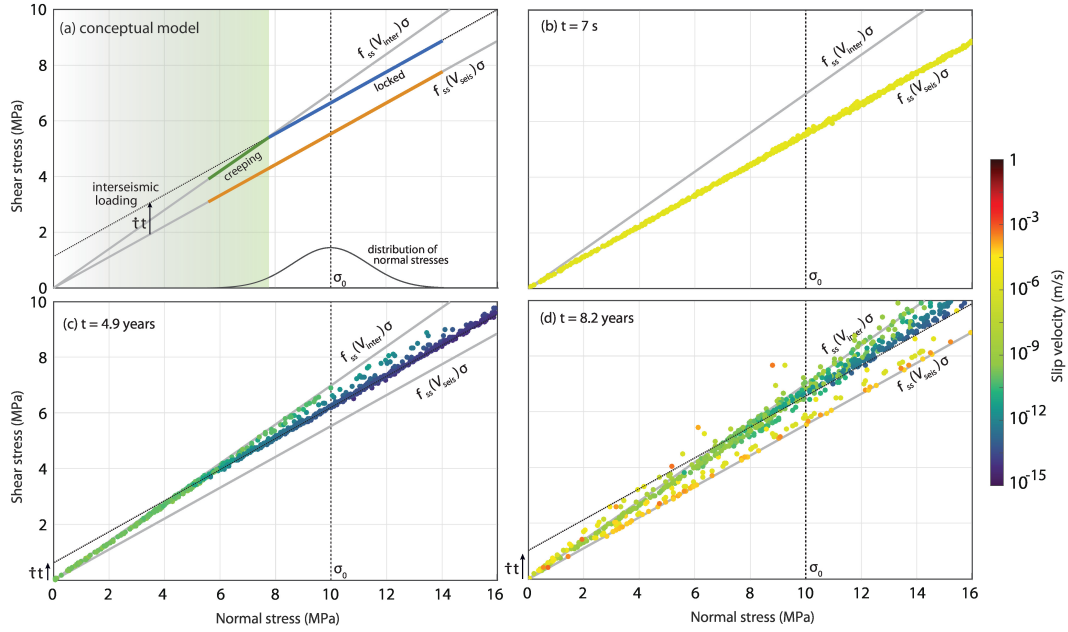


Figure 3. Conceptual model and simulation results for the evolution of stress on the fault.

(a) Expected state of stress after the entire fault has ruptured (orange) and later in the cycle: points at low σ reach the end of their cycle first and start creeping (green), while asperities are still locked (blue). σ_0 is the unperturbed normal stress, and a Gaussian distribution of σ due to slip (as derived in Appendix A) is shown in black. The grey lines indicate the static and dynamic strength (i.e. the steady-state strength at interseismic and coseismic slip velocities respectively).

(b-d) Shear and normal stresses from the simulation, right after an earthquake (b); during the aseismic phase of the cycle (c); towards the end of the nucleation phase (d).

193 fractal fault with Hurst exponent H , its standard deviation is given by

$$\Delta\sigma_{rms} = \frac{\mu'\alpha S}{2} \sqrt{\frac{H}{2-H}} (2\pi)^H k_{max}^{2-H}, \quad (10)$$

194 where $\mu' = \mu/(1 - \nu)$ and ν is Poisson's ratio and α the roughness, which quantifies
 195 the amplitude of topography such that the root-mean-square elevation measured over
 196 a length l is given by $y_{rms} = \alpha l^H$ (section A1). These variations in normal stress are
 197 responsible for the occurrence of alternating creeping and locked regions, as shown in
 198 Fig. 4: creep takes place where roughness decreases the normal stress, while regions with
 199 increased σ remain locked.

200 A simple model illustrating the heterogeneous response of a rough fault loaded at
 201 uniform shear stressing rate is shown in Fig. 3. After a system-wide rupture, all points
 202 on the fault are at steady-state friction $f_{co} = f_{ss}(V_{co})$, given by eq. 4, with V_{co} the seis-
 203 mic slip velocity (this applies if fault healing occurs on a much longer timescale than the
 204 earthquake itself, as in the case of the ageing rate-state friction). As the fault is loaded
 205 at a uniform stressing rate, points with low σ reach “static” strength sooner than those
 206 at high σ (Fig. 3(a)). A creeping patch may then become unstable if it exceeds a crit-
 207 ical elasto-frictional length, or creep at constant stress otherwise. The steady-state ve-
 208 locity is $V_{cr} = \dot{\tau}/\kappa$, where κ is the stiffness, which for a region of size L is of the or-
 209 der of μ'/L so that $V_{cr} \approx L\dot{\tau}/\mu'$. The critical length for instability (nucleation length)
 210 was first estimated from a spring-slider linear stability analysis (Ruina, 1983); later, Rubin
 211 and Ampuero (2005) used energy balance arguments to derive expressions for ageing rate-
 212 state faults. In general, this critical length has the form

$$L_c = f(a, b) \frac{\mu' d_c}{\sigma} \quad (11)$$

214 where $f(a, b)$ is a function of rate-state parameters a, b ; for rate-state friction with the
 215 ageing law and $a/b = 0.75$ (as in our case), $f(a, b) = b/[\pi(b - a)^2]$ and the nucleation
 216 length is denoted by L_∞ (Rubin & Ampuero, 2005). Expressions for nucleation length
 217 derived for a homogeneous fault cannot directly be applied to an heterogeneous one. How-
 218 ever, linear fracture mechanics can be used to derive alternative expressions for these cases,
 219 as done by Tal et al. (2018) for rough faults with small scale (sub- L_c) roughness, and Dublan-
 220 chet (2018) for heterogeneous friction. With these caveats in mind, here we appeal to the con-
 221 cept of an heterogeneous nucleation length as an intuitive way to relate spatial variations
 222 in normal stress to slip behavior.

223 Due to the inverse proportionality between L_c and σ , the first patches to reach static
 224 strength are the most stable ones (large L_c), thus favouring stable creep. During this phase
 225 we expect the average slip velocity on the fault to increase for several reasons: 1) the area
 226 of creeping patches increases as more points reach static strength, since the time to fail-
 227 ure is given by $T_f \simeq \Delta\tau/\dot{\tau}$, where $\Delta\tau = [f_{ss}(V_{co}) - f_{ss}(V_{cr})]\sigma$ is the difference be-
 228 tween the dynamic and static strength (Fig. 3); 2) Creep on low σ patches redistribute
 229 stresses onto locked patches, contributing to the acceleration by causing points to be closer
 230 to failure than predicted from tectonic loading in Fig. 3(c); 3). The steady state slip ve-
 231 locity on each patch increases as it widens, since the average slip velocity in the creep-
 232 ing regions $V_{cr} \sim L_{cr}$ where L_{cr} is the dimension of creeping patches. This leads to the
 233 interseismic acceleration seen in Fig. 1. As creep occurring in low σ regions penetrates
 234 into asperities, it can cause them to fail in localized slow slip or earthquakes (velocity
 235 peaks in Fig. 1). Microseismicity occurs late in the cycle since the most locked patches,
 236 where the nucleation length is small enough to allow seismic rupture, are the last to reach
 237 failure.

238 5 Seismicity on strong patches

239 Foreshocks occur in subclusters at multiple temporal scales: Figs. 2 and 4 show 3
 240 events occurring a few days before the mainshock, followed by quiescence and a second
 241 cluster about a day later; more clusters occur a few hours and a few minutes before the
 242 mainshock. Each burst represents the rupture of a group of nearby asperities (Fig 4 and
 243 Supplementary Figure S2), and the relative location of each event is consistent with static
 244 stress transfer from previous ones. This gives rise to migration (e.g. events 1-8, 9-14),
 245 which can also reverse due to repeated rupture of the same asperity (e.g. events no. 1,13,14
 246 and 2,12,14 among others). Seismic clusters are bounded by stronger or wider asperi-
 247 ties, which typically fail in later bursts: the increase in shear stress imparted by earth-
 248 quakes on surrounding low σ patches leads to a sudden creep acceleration, which in turn
 249 loads nearby asperities until they fail (see for example accelerated creep at the edge of
 250 previous foreshocks leading up to events 6, 11 and 14 in Fig. 4). Similarly, the mainshock
 251 initiates at the edge of the previous events and the creeping region. The asperity on which
 252 it nucleates has a higher normal stress than nearby asperities and previous foreshocks.

253 In spite of the elevated normal stress on asperities, foreshocks don't have partic-
 254 ularly high stress drops (0.1-2MPa): in agreement with Schaal and Lapusta (2019), who

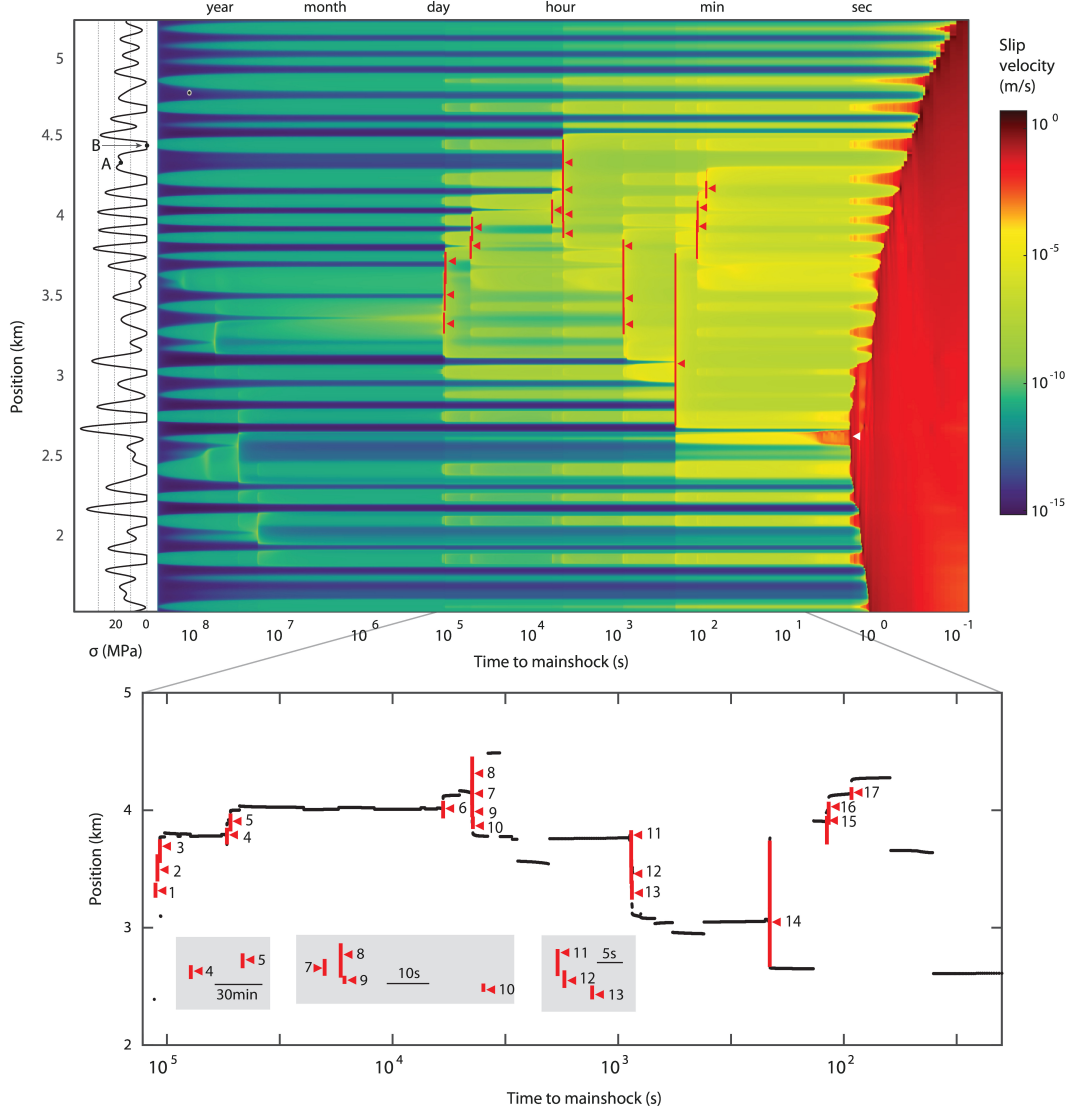


Figure 4. Creep acceleration and seismicity leading up to a mainshock. Top: slip velocity on the fault vs. time to the end of the mainshock, with red bars marking the rupture length and triangles marking the nucleation point (mid-point of the region where $v > V_{dyn}$ during the first earthquake time step). The inset on the left shows normal stress at the beginning of this cycle. Note the sudden acceleration in nearby creeping patches and the widening of the fast slipping region with each successive seismic burst. The instantaneous localized accelerations seen at $\sim 3 - 5$ km, just before the arrival of the mainshock front are a consequence of the model assuming instantaneous stress changes. Bottom: subset of the top panel, with events numbered by occurrence time. Small black dots and lines indicate the location of maximum slip velocity at each time step, showing accelerated creep at the edges of each burst, where the subsequent ones initiate. Grey panels show close ups of a few clustered foreshocks.

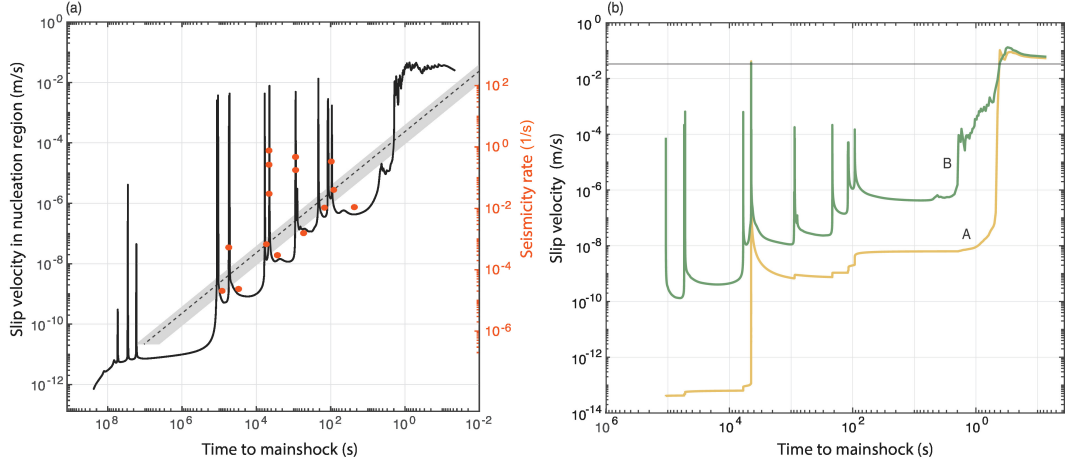


Figure 5. Slip velocity and seismicity rates during the foreshock sequence shown in Fig. 4. (Left) Black solid line: average slip velocity in the mainshock nucleation region (between 2.2km and 4.5km) vs. time to the end of the mainshock. Red circles: seismicity rates estimated by the inverse of interval times, plotted at the midpoint between each pair of events. The y-axes are scaled with respect to one another according to eq. C1. The theoretical evolution of slip velocity (eq. 14) is indicated by the dotted line (for the median value of foreshock stress drop) and grey band (for the entire range of stress drops). (Right) Slip velocity vs. time for the asperity (A) and a nearby creeping patch (B), which are identified on Fig. 4. The horizontal line indicates the threshold velocity V_{dyn} used to identify earthquakes.

255 observed a similar behavior in 3-D simulations, we find that foreshocks are not confined
 256 to asperities, but propagate into the surrounding low σ regions, thus lowering the av-
 257 erage stress drop. The presence of such low stress-drop regions is also responsible for the
 258 partial overlap between consecutive events, even though in some cases asperities them-
 259 selves rerupture (Fig. 4).

260 5.1 Feedback between creep and foreshocks

261 The average slip velocity during the foreshock sequence increases in sudden steps
 262 after failure of one more asperities (Fig. 4, 5a). The acceleration occurs even at large dis-
 263 tances from the foreshocks compared to their rupture dimension, so that foreshocks con-
 264 tribute to widening the fast creeping area. Average slip velocities on the fault increase
 265 approximately with the inverse of time to mainshock (Fig. 5), similar to studies of ve-
 266 locity weakening asperities embedded in a velocity strengthening (creeping) fault (Dublan-
 chet,

267 2018; Yabe & Ide, 2018). However, neither asperities nor creeping patches follow this trend
 268 individually (Fig. 5b).

269 To understand the effect of a seismic rupture on weak patches, consider the change
 270 in velocity caused by an instantaneous shear stress perturbation $\Delta\tau$ through the direct
 271 effect:

$$V = V_0 e^{\Delta\tau/a\sigma}, \quad (12)$$

272 where V_0 is the starting velocity. For a given stress change, areas at low normal stress
 273 are particularly susceptible to stress increases due to foreshocks, even if they are several
 274 rupture lengths away. As an example, Fig. 5(b) shows slip velocities on the asperity which
 275 ruptured in a foreshock (event no.8 in Fig. 4) and a nearby creeping patch, marked in
 276 Fig. 4. After the earthquake, the asperity does not fully relock, but continues slipping
 277 about 4 orders of magnitude faster than it did before. This behavior can be explained
 278 by the faster loading rate from the nearby creeping patches, which prevents the asperity
 279 from fully relocking. We can gain some intuition into this by treating the asperity
 280 as a spring-slider driven at a constant stressing rate, which in turn depends on the creep
 281 rate around it. The solution for velocity evolution derived in Appendix B predicts that
 282 the minimum slip speed right after an earthquake grows with stressing rate $\dot{\tau}$:

$$V_{lock} = V_{dyn} e^{b/a} \left(\frac{d_c \dot{\tau}}{b\sigma V_{dyn}} \right)^{b/a}. \quad (13)$$

283 After a mainshock, $\dot{\tau} \approx \dot{\tau}_0$ (the background loading rate); during the nucleation phase,
 284 creep velocities adjacent to the asperities increase (in this case, $V_{cr} \sim 1 \times 10^{-8}$ m/s;
 285 see Fig.5), giving a stressing rate on the asperity of the order of $\dot{\tau}_{cr} \approx \mu' V_{cr} / L_{asp} \approx$
 286 $\mu' V_{cr} / L_{min} = 4$ Pa/s, here about 10^3 times larger than the background loading rate $\dot{\tau}_0$.
 287 Plugging these numbers in the expression above, we expect V_{lock} after the foreshock to
 288 be about $\sim 10^4$ times larger than its minimum value early in the cycle, consistent with
 289 the simulation (Fig. 5). The creeping patches and asperities subsequently decelerate,
 290 but the asperity slip velocity remains several orders of magnitude larger than before rup-
 291 ture (Fig. 4, 5).

292 The positive feedback between creep rates and seismicity rates leads to an over-
 293 all acceleration and expansion of the creeping region. In Appendix C we derive a sim-
 294 ple analytical expression based on the observations described above. It relies on the fol-
 295 lowing assumptions: 1. seismicity rate is proportional to average creep rate; 2. creep rates
 296 increase by a constant factor after each foreshock (derived from eq. 12), and don't change

297 otherwise. This simple model predicts that the average slip velocity evolves as

$$\langle V \rangle = \frac{2L_{min}^2 \Delta\tau}{L\mu' \log(\beta)} \frac{1}{t_0 - t} \quad (14)$$

298 where L is the dimension of the nucleation region, $\Delta\tau$ the foreshock stress drop and β
 299 a factor quantifying the increase in creep velocity after each foreshock; t is time since the
 300 first foreshocks and t_0 the time to instability, given by

$$t_0 = \frac{2L_{min}^2 \Delta\tau}{L\mu' \log(\beta) \langle V_0 \rangle}. \quad (15)$$

301 We estimated β by applying eq. 12 to the creep patches in the nucleation region, and
 302 treating foreshocks as uniform stress drop cracks of fixed size, and we obtained values
 303 between 1.1–1.3 (the range is given by variability in foreshock stress drops). Overall,
 304 the average slip velocity in the nucleation region increases approximately as predicted
 305 by this expression (Fig. 5a).

306 5.2 Stacked foreshock and aftershock catalogs

307 The prediction of $1/t$ acceleration in creep rates and seismicity rates does not ac-
 308 count for temporal clustering due to elastic interactions between asperities, visible in Fig. 5.
 309 Therefore, the $1/t$ acceleration in seismicity rates may not be readily visible in individ-
 310 ual catalogs. To better capture temporal patterns, we stack the catalogs from all cycles.
 311 All foreshocks-aftershock sequences are shifted so the mainshock occurs at $t = 0$, and
 312 then combined in a single catalog. As shown in Fig. 6(a), the rate of foreshocks increases
 313 with the inverse time to the mainshock, as observed for stacked catalogs of natural se-
 314 quences (Jones & Molnar, 1979; Ogata et al., 1995).

315 5.3 Onset of foreshocks and mainshock

316 The occurrence of foreshocks in the vicinity of the mainshock hypocenter raises the
 317 following question: why do some ruptures arrest, while others in the same region grow
 318 into large events? Fig. 4 shows that the mainshock, like most foreshocks, nucleates at
 319 the edge of a fast creeping region, on an asperity which arrested the previous event. The
 320 mainshock nucleation asperity has the highest normal stress on the entire fault. To ver-
 321 ify whether other mainshocks also nucleate on high σ asperities, we compare normal stresses
 322 in the nucleation region of mainshocks and nearby foreshocks. Fig. 7 shows that main-
 323 shocks tend to nucleate on stronger asperities than most of their foreshocks. This may

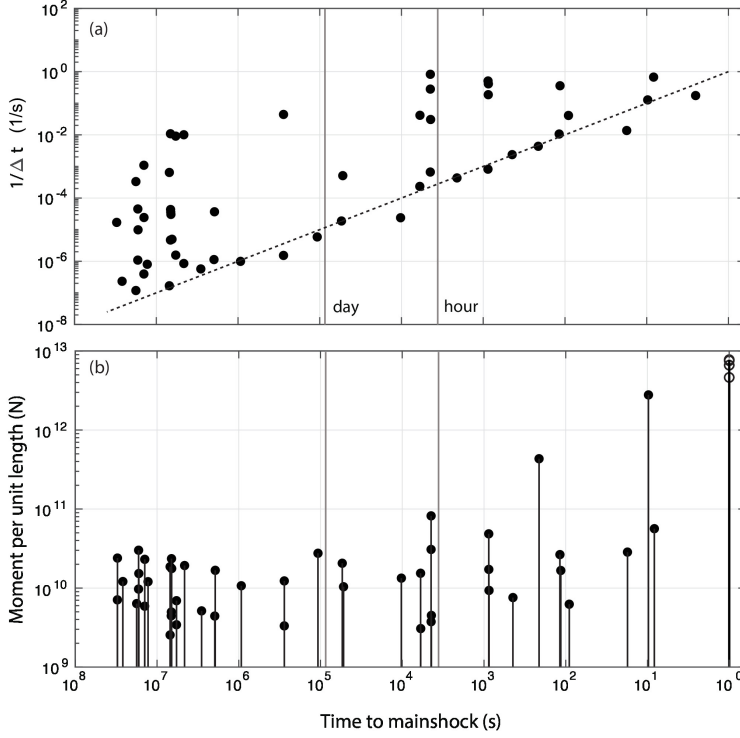


Figure 6. Moment per unit length and interevent times in the stacked catalog. (a) Seismicity rates estimated as the inverse of interevent time showing power-law acceleration. The dotted line is proportional to $1/t$. (b) moment per unit length as a function of time to mainshock. Open circles indicate mainshocks.

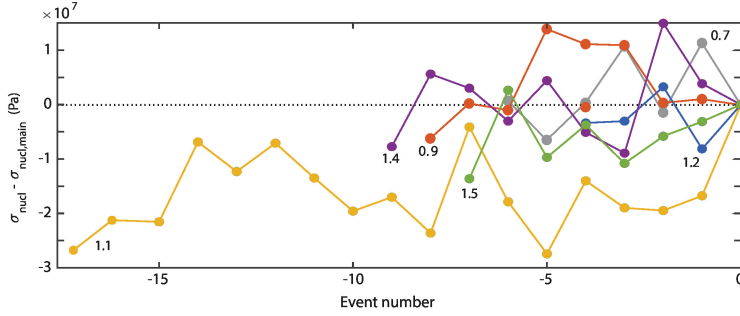


Figure 7. Difference between average normal stress in the nucleation region of foreshocks and their respective mainshocks. Nucleation is defined as the region between points exceeding a velocity threshold at the beginning of an earthquake (see section 2). We consider mainshocks as events with a rupture length exceeding 2km, and only select foreshocks within the mainshock rupture area. Numbers indicate $\Delta\sigma_{rms}/\sigma_0$ for each sequence.

324 not be surprising in light of the simple model shown in Fig. 3, since patches with higher
 325 normal stress take longer to reach static strength. Once a strong asperity breaks, its stress
 326 drop is high and leads to a more pronounced stress concentration at its edge, allowing
 327 it to grow further than earlier events. This also explains why larger foreshocks tend to
 328 occur later in the cycle (Fig. 6(b)).

329 Rupture arrest is also determined by the strength of asperities ahead of the rup-
 330 ture tip, which act as barriers. We consider all asperities which are either within or ad-
 331 jacent to a rupture, and as expected we find that stronger (higher normal stress) asper-
 332 ities are more likely to arrest ruptures. We also find that a rupture nucleating at nor-
 333 mal stress σ_{nuc} has a 62% probability of breaking an asperity with normal stress exceed-
 334 ing σ_{nuc} , and a 77% chance of breaking an asperity with normal stress lower than σ_{nuc} .
 335 A selection bias could originate when grouping asperities according to this criterion: on
 336 average, asperities with $\sigma_{asp} > \sigma_{nuc}$ for a given earthquake are stronger than those with
 337 $\sigma_{asp} < \sigma_{nuc}$. However, we find that a difference remains when comparing asperities with
 338 approximately the same normal stress, indicating that σ_{nuc} also affects rupture arrest.

339 6 Discussion

340 The results presented above show that the preseismic phase on a velocity-weakening
 341 fault with fractal roughness is characterized by a complex interplay between slow slip
 342 and foreshocks. Most of the period between mainshocks is devoid of seismicity, and char-
 343 acterized by localized patches of slow slip; late in the cycle, strong asperities start fail-
 344 ing in short bursts, each of them in turn accelerating creep in its neighbourhood. This
 345 process leads to acceleration over an extended region (here about 20 times larger than
 346 the nominal nucleation dimension), with migration of seismicity towards the mainshock
 347 hypocenter.

348 6.1 Model limitations

349 The central result of this study is the coexistence and interaction of slow slip and
 350 foreshocks during nucleation on a rough fault. The primary control on this mixed be-
 351 havior are normal stress perturbations due to roughness, and their effect on fault sta-
 352 bility and slip patterns (section 4). These findings are not specific to rate-state (ageing
 353 law) friction, and likely apply for other frictional laws and weakening mechanism. On
 354 the other hand, certain simplifications in our study may be more consequential and de-

355 serve further investigation. The quasi-dynamic approximation can affect rupture veloc-
 356 ity, rupture arrest and lengths, even though based on previous planar fault studies (Lapusta
 357 et al., 2000; Thomas et al., 2014) we don't expect the qualitative pattern to change dra-
 358 matically with ageing-law rate-state friction. Considering the 3-dimensional nature of
 359 fault surfaces can modify certain aspects of fault dynamics, such as the ability of an as-
 360 perity to arrest rupture or the migration patterns caused by stress redistribution. In par-
 361 ticular, static stress changes extend further in 2D than 3D. Another significant assump-
 362 tion in our study is the purely elastic response: inelastic processes would limit the am-
 363 plitude of stress perturbations, in particular at the smallest length scales (e.g. Dunham
 364 et al., 2011).

365 6.2 Conditions for foreshock occurrence

366 The dimension of asperities relative to characteristic elasto-frictional length scales
 367 is expected to affect foreshock behavior. Previous numerical studies of foreshocks on het-
 368 erogeneous faults found that foreshocks only occur in a particular regime (Schaal & La-
 369 pusta, 2019; Dublanchet, 2018): asperities must be larger than the local nucleation di-
 370 mension for seismic slip to occur, but smaller than a critical dimension (such as the nu-
 371 cleation dimension outside the asperity) to arrest without generating system-size rup-
 372 tures. Here, the amplitude of spatial variations in σ controls the range of local nucleation
 373 lengths L_c . As more slip accrues and normal stress perturbations grow, the nucleation
 374 length shrinks on the asperities and grows around them: therefore microseismicity only
 375 appears for sufficiently large normal stress perturbations (here $\Delta\sigma_{rms} \approx \sigma_0$).

376 A similar transition from few large ruptures to many smaller ones was found by Heimisson
 377 (2020) when increasing k_{max} ; since the amplitude of normal stress perturbations grows
 378 with k_{max} (eq. 10), this is consistent with our findings. Similarly, we expect that increas-
 379 ing fault roughness would have the same effect, since $\Delta\sigma_{rms}$ increases with the product
 380 of roughness and accrued slip. In our simulations, we chose $k_{max} \sim 2\pi/L_\infty$, for com-
 381 putational efficiency. To verify the effect of smaller wavelengths, we also ran simulations
 382 for a smaller domain and k_{max} up to 4 times higher (Supplementary Figure 2). We find
 383 that the presence of sub- L_∞ asperities leads to more frequent aseismic ruptures (sim-
 384 ilar to those in Fig. 1). Both seismic and aseismic failures contribute to a gradual un-
 385 pinning of the fault, as described above. The temporal evolution of slip velocities, with

386 an abrupt increase during bursts and an overall $1/t$ trend, is similar to the nominal
 387 case.

388 **6.3 Preslip vs. nucleation on rough faults**

389 In the “preslip” model, aseismic slip is generally understood to occur at the loca-
 390 tion of the mainshock hypocenter, reflecting the notion that seismic instabilities develop
 391 over a region of finite size, as predicted by spring slider and continuum models (e.g. Ru-
 392 ina, 1983; Rubín & Ampuero, 2005). It is conceivable that heterogeneity *within* the nu-
 393 cleation region could lead to foreshocks driven by accelerating slip (e.g. Noda et al., 2013);
 394 however, our results favor a different interpretation. Here the large scale precursory ac-
 395 celerating slip is not mainshock nucleation in the classical sense: since slow slip occurs
 396 in stable low σ patches which do not accelerate when subject to slow loading, it does not
 397 directly evolve into a seismic rupture. Instead, slow slip triggers smaller scale nucleation
 398 on locked asperities, which can remain small or grow into a mainshock.

399 A similar relationship between preslip and mainshock initiation in presence of het-
 400 erogeneity has been inferred in laboratory experiments. McLaskey and Lock-
 401 ner (2014) observed acoustic emissions (analogous to foreshocks) and slow slip leading
 402 up to failure in a centimeter-scale laboratory sample, and noted that system-size rup-
 403 tures begin as acoustic emissions, with local strength variations perhaps controlling whether
 404 they evolve into larger ruptures. Similarly, meter-scale experiments by McLaskey (2019)
 405 show evidence of abrupt earthquake initiation caused by creep penetration from weak
 406 regions into a locked patches, “igniting” large ruptures.

407 The migratory behavior of microseismicity, and the earthquake hypocenter on the
 408 edge of the creeping region, also indicate of a different mechanism than self-nucleation.
 409 Recent observations of precursory slip leading up to glacial earthquakes by Barcheck et
 410 al. (2021) are similar to our results: slow slip and microseismicity migrate towards the
 411 mainshock hypocenter. Similar seismicity migration has also been observed prior to sev-
 412 eral events (Tohoku, 2011, A. Kato et al. (2012); Iquique, Brodsky and van der Elst (2014);
 413 l’Aquila, Sukan et al. (2014)), and it is sometimes interpreted as evidence for aseismic
 414 slip.

415 On the other hand, migratory behavior can also be interpreted as evidence for di-
 416 rect triggering between foreshocks: seismicity prior to the 1999 Izmit (Ellsworth & Bu-

417 lut, 2018) and 1999 Hector Mine (Yoon et al., 2019) exhibit a cascade behavior similar
418 to that observed here (Fig. 4): successive failure of neighbouring asperities, with each
419 event nucleating at the edge of the previous ones, and in one case a rerupture of the same
420 asperity (as in Fig. 4). Here, we find that the migration is in some cases caused by di-
421 rect stress triggering (leading to rapid failure of nearby asperities in a short burst), but
422 it can also be mediated by accelerated creep between asperities. Note that direct stress
423 transfer between asperities would be less effective in 3-D, and aseismic slip is therefore
424 likely to play a more important role in this geometry (see also Lui and Lapusta (2016)).

425 Stacked earthquake catalogs exhibit a gradual power-law acceleration (Jones & Mol-
426 nar, 1979; Ogata et al., 1995; Bouchon et al., 2013), analogous to Fig. 6. However, in-
427 dividual sequences typically display more irregular patterns: Chen and Shearer (2013)
428 observed burst-like behavior for foreshock sequences in California, and A. Kato, Fukuda,
429 Kumazawa, and Nakagawa (2016) documented abrupt changes in seismicity and aseis-
430 mic slip prior to the 2014 Iquique earthquake. A gradual $1/t$ acceleration is predicted
431 by spring-slider models of nucleation on rate-state faults (Dieterich, 1992; Rubin & Am-
432 puero, 2005); on the other hand, Helmstetter and Sornette (2003) derived the same re-
433 sults from earthquake triggering with foreshocks producing offspring at a rate given by
434 the Omori-Utsu law, without requiring aseismic slip, and Felzer et al. (2015) invoked the
435 same mechanism to explain the apparent acceleration prior to large interplate earthquakes.
436 Here we suggest that both processes are at play, and demonstrate that a $1/t$ acceleration
437 can arise from the interaction of seismic failure on isolated asperities and the surround-
438 ing creeping regions. Unlike seismicity driven by gradually accelerating slow slip, in this
439 case both earthquake rates and slip velocities increase in abrupt steps, so that the power-
440 law behavior is visible for stacked catalogs but not for individual sequences.

441 An intriguing observation is the occurrence of earthquakes in the vicinity of a fu-
442 ture mainshock hypocenter. The 2004 M_w 6 Parkfield and the M_w 9 Tohoku earthquakes
443 were both preceded by moderate events within a few years of the mainshock, a much shorter
444 timescale than the respective earthquake cycles. Based on our results, which should be
445 further verified with fully dynamic simulations, we suggest that local strength variations
446 between potential nucleation patches within a small region may determine which earth-
447 quakes evolve into destructive events.

7 Conclusions

We find that fault roughness can lead to simultaneous occurrence of aseismic slip and foreshocks in the precursory phase of mainshocks, modulated by normal stress variations caused by fault geometry. The precursory phase can be described as a gradual unpinning of the fault by episodic asperity failure, mediated by aseismic slip. The creeping area widens and accelerates through each seismic burst, leading to migration of seismicity towards the eventual mainshock hypocenter. A simple model for the positive feedback between creep and seismicity predicts that slip accelerates as $1/t$, as confirmed by the simulations.

This process results in precursory slip on a larger scale than, and spatially distinct from, classical rate state nucleation on flat faults. Our results provide a physical interpretation for laboratory and field evidence of migratory preslip and foreshocks in the vicinity of a future mainshock hypocenter.

Appendix A Normal stress variations

Here we derive the spatial distribution of normal stresses due to slip on a rough fault with small perturbations in elevation $y(x)$ (i.e., distance from the mean fault position). Fang and Dunham (2013) derived the following expression for normal stress perturbations due to uniform unit slip:

$$\Delta\sigma(x) = \frac{\mu'}{2\pi} \int_{-\infty}^{\infty} \frac{y''(\xi)}{x - \xi} d\xi \quad (\text{A1})$$

where $\mu' = \mu/(1 - \nu)$ and compressive stresses are positive. The elevation profile can be written as

$$y(\xi) = \int_{k_{min}}^{k_{max}} \hat{y}(k) e^{ik\xi} dk \quad (\text{A2})$$

Taking the second derivative and inserting into eq. A1 gives

$$\begin{aligned} \Delta\sigma(x) &= \frac{\mu'}{2\pi} \int_{-\infty}^{\infty} \frac{1}{\xi - x} \int_{k_{min}}^{k_{max}} k^2 \hat{y}(k) e^{ik\xi} dk d\xi \\ &= \frac{\mu'}{2\pi} \int_{k_{min}}^{k_{max}} k^2 \hat{y}(k) e^{ikx} \int_{-\infty}^{\infty} \frac{1}{u} e^{iku} du dk, \end{aligned}$$

where $u = \xi - x$. We use the following results:

$$\begin{aligned}
474 \quad & \int_{-\infty}^{\infty} \frac{\sin(kx)}{x} dx = \pi \\
475 \quad & \int_{-\infty}^{\infty} \frac{\cos(kx)}{x} dx = 0.
\end{aligned}$$

476

477 Thus, the inner integral takes the value of $i\pi$ and

$$478 \quad \Delta\sigma(x) = \frac{\mu' S}{2} \int_{k_{min}}^{k_{max}} k^2 \hat{y}(k) e^{i(kx+\pi/2)} dk, \quad (\text{A3})$$

479 where we have scaled the stress by the total slip S . The integral has a form similar to
480 the second derivative of the topography, but with a phase shift of $\pi/2$ in each Fourier
481 component. This result is consistent with the findings of Romanet et al. (2020), who
482 demonstrated that normal stress perturbations on a curved fault are proportional to the
483 local curvature (which to first order is equal to the second derivative of the slope). The
484 phase shift can be intuitively understood by considering a sinusoidal profile: a phase shift
485 of $\pi/2$ places maximum compressive and tensile stresses at the inflection point of restrain-
486 ing and releasing bends (see fig. A1). Since stress perturbations depend on the second
487 derivative of the elevation profile, they are dominated by the shortest wavelengths.

488 We emphasize that in the simulations normal stress perturbations are not prescribed
489 or computed by the above expressions. Rather they arise in the boundary element cal-
490 culations from stress transfer between elements with variable orientation (section 2). Nev-
491 ertheless, the analytical result may prove useful to approximate the effect of roughness
492 by imposing normal stress perturbations on a planar fault (e.g. Schaal & Lapusta, 2019),
493 even though this method would not account for the increase in perturbations with slip.

494 Roughness also affects shear stresses on the fault. The two are related by eq. 1, which
495 during most of the cycle can be approximated as $\tau_{el} \approx f\sigma$ (and since with rate-state
496 friction fractional changes in f are small compared to σ , $\tau_{el} \approx f_0\sigma$). Equilibrium is achieved
497 by a heterogeneous slip distribution modulating stresses. On a fault with small devia-
498 tions from planarity, slip gradients efficiently modify shear stresses, but have little ef-
499 fect on normal stresses (this can be understood intuitively from the fact that slip on a
500 planar fault has no effect on σ ; for a more general derivation, see Romanet et al. (2020)).
501 Therefore, roughness induced variations in τ are accommodated by slip gradients, while

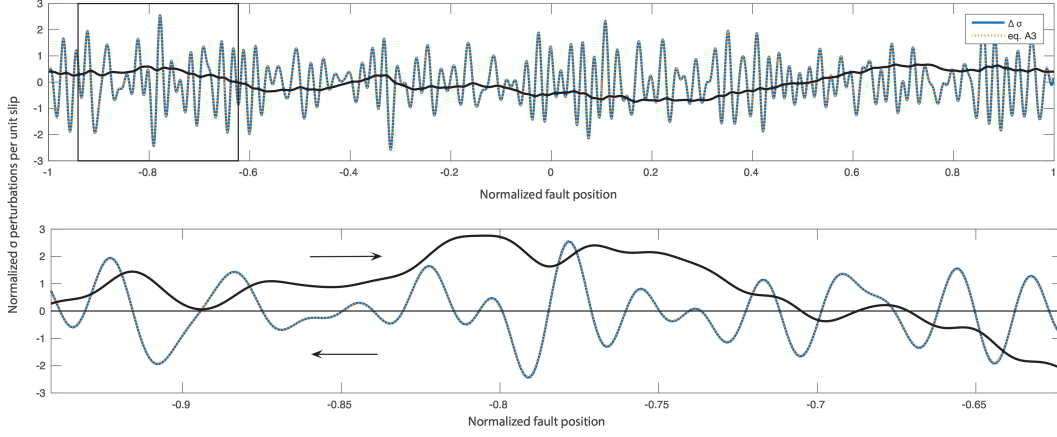


Figure A1. Top: Normal stresses from BEM calculations used in FDRA (blue) and eq. A3 (dotted yellow), as a function of normalized position, with unit slip, normalized by $\mu'/2$. Black: fault profile rescaled by a factor of 500. Bottom: zoomed in (inset in top figure), with fault profile scaled by 4000, showing normal stress perturbations corresponding to releasing and restraining bends.

502 the normal stress distribution remains virtual unchanged between large earthquakes and
 503 determines the shear stress profiles.

504 **A1 Self-similar roughness**

505 Consider a fault with a profile y characterized by power spectral density

$$506 \quad P_h = C_h |k|^{-\beta} \quad (\text{A4})$$

507 between $k_{min} = 2\pi/L$ and k_{max} , with $\beta = 2H + 1$ and H the Hurst exponent. Using
 508 Parseval's theorem it can be shown that the root mean square elevation in the limit $k_{max} \gg$
 509 k_{min} is

$$510 \quad y_{rms} = \sqrt{\frac{C_h}{\pi(\beta-1)}} \left(\frac{L}{2\pi}\right)^H = \alpha L^H \quad (\text{A5})$$

511 where α is the surface roughness. Similarly, by applying Parseval's theorem to the sec-
 512 ond derivative of y we obtain the the root mean square value:

$$513 \quad y''_{rms} = \alpha \sqrt{\frac{H}{2-H}} (2\pi)^H k_{max}^{2-H} \quad (\text{A6})$$

514 Here we used fractal surfaces with random phases, resulting in a Gaussian distri-
 515 bution in $y(x)$; $y''(x)$ is also Gaussian with standard deviation y''_{rms} (e.g. Persson et al.,
 516 2005). Combining this result with eq. A3, we find that normal stress perturbations are
 517 Gaussian distributed with zero mean and standard deviation $\mu' S y''_{rms}/2$, where S is the
 518 accrued slip.

519 Appendix B Spring slider

520 To obtain the interseismic evolution of slip velocity, we consider a spring-slider with
 521 stiffness κ driven at constant rate $\dot{\tau}_L$:

$$522 \quad \frac{\tau_0 + t\dot{\tau}_L - \kappa\delta}{\sigma} = [f_0 + a \ln(V/V^*) + b \ln(\theta V^*/d_c)] , \quad (B1)$$

523 where δ is slip and τ_0 is shear stress at time $t = 0$ (see also Rubin and Ampuero (2005),
 524 eq.A12). Since we are interested in the velocity during the interseismic phase, the ra-
 525 diation damping term is not included. Time is measured since the last earthquake, and
 526 τ_0 is the residual stress after rupture. More specifically, we define $t = 0$ as the moment
 527 when the system last crossed steady-state, and

$$528 \quad \frac{\tau_0}{\sigma} = f_0 + (a - b) \log(V_{dyn}/V^*) \quad (B2)$$

529 with V_{dyn} as defined in section 2. Inserting eq. B2 into eq. B1 and solving for V gives

$$530 \quad V(t) = V_{dyn} \exp\left(\frac{t\dot{\tau}_L - k\delta}{a\sigma}\right) \left(\frac{d_c}{\theta V_{dyn}}\right)^{b/a} . \quad (B3)$$

531 Further assuming that the fault is locked ($k\delta/a\sigma \ll 1$) and far below steady-state ($\theta \sim$
 532 t), velocity evolves as

$$533 \quad V(t) = V_{dyn} \exp\left(\frac{t\dot{\tau}_L}{a\sigma}\right) \left(\frac{d_c}{tV_{dyn}}\right)^{b/a} . \quad (B4)$$

534 The minimum velocity occurs at $t = b\sigma/\dot{\tau}_L$ and is given by

$$V_{lock} = V_{dyn} e^{b/a} \left(\frac{d_c \dot{\tau}_L}{b\sigma V_{dyn}}\right)^{b/a} . \quad (B5)$$

Appendix C Preseismic acceleration

As discussed in section 5.1, the acceleration leading up to the mainshock is controlled by a feedback between creep in low normal stress patches and foreshocks on asperities. Here we develop a simple model of these interactions and the temporal evolution of acceleration.

Seismicity rate is controlled by the surrounding creep rate, which for simplicity we take as uniform. The interevent time on a single asperity is of the order of $\Delta\tau/\dot{\tau}$, where $\Delta\tau$ is the stress drop. Note that this expression does not apply if some interseismic slip takes place within the rupture area; however, Cattania and Segall (2019) obtained a similar expression, within a factor of order one, allowing for creep to penetrate the asperity. The overall seismicity rate on the fault is therefore $N\dot{\tau}/\Delta\tau$, where $N \approx L/L_{min}$ is the number of asperities in a nucleation region or length L . During nucleation we can neglect tectonic loading, so $\dot{\tau} \approx \dot{\tau}_{cr} = \kappa V(t)$, with $\kappa \sim \mu'/2L_{min}$ so that the seismicity rate is

$$\frac{dn}{dt} = \frac{L \mu'}{2L_{min}^2 \Delta\tau} \langle V \rangle. \quad (C1)$$

where n is the cumulative number of foreshocks, and $\langle V \rangle$ denotes average slip velocity. We further assume that each earthquake increases the average creep rate by a constant factor β , derived below, and we neglect self-acceleration of creeping patches. Slip velocities are then given by

$$\langle V(n) \rangle = \langle V_0 \rangle \beta^n \quad (C2)$$

where V_0 is the average slip velocity before the first foreshock. Differentiating eq. C2 and combining with eq. C1 results in

$$\frac{d\langle V \rangle}{dt} = \frac{L\mu' \log(\beta)}{2L_{min}^2 \Delta\tau} \langle V \rangle^2 \quad (C3)$$

which has solution

$$\langle V \rangle = \frac{2L_{min}^2 \Delta\tau}{L\mu' \log(\beta)} \frac{1}{t_0 - t} \quad (C4)$$

where t is time since the first foreshocks and t_0 the time to instability, given by

$$t_0 = \frac{2L_{min}^2 \Delta\tau}{L\mu' \log(\beta) \langle V_0 \rangle}. \quad (C5)$$

Note that we assumed that the creep velocity remains high after each foreshock. For a creep patch of fixed dimension (stiffness) subject to a sudden stress increase, we would

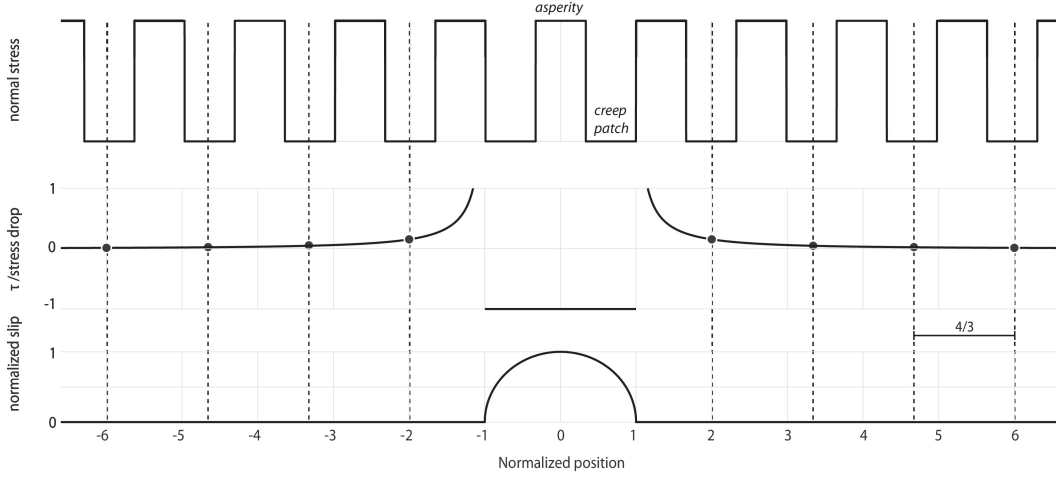


Figure C1. Simple model used to estimate changes in creep rate after a foreshock. Top: schematic spatial distribution of normal stress. Middle: shear stress change caused by a constant stress drop crack normalized by stress drop. Bottom: foreshock slip distribution. Dotted lines and circles indicate the center of creeping patches and locations at which stress changes are calculated.

559 instead expect velocity to decay to the steady-state value determined by the background
 560 loading rate; however, simulations show that creep velocities remain high after each step
 561 (Fig. 4, 5), possibly due to the reduction in stiffness after each foreshock described in
 562 section 5.1.

563 The functional form of eq. C1 and C2 is not expected to change in 3D (even though
 564 β and the prefactor in eq. C1 will differ). Therefore we expect the main result of this
 565 analysis, which is the growth of velocity as the inverse of time to instability, to remain
 566 valid.

567 **C1 Estimating β**

568 To obtain a rough estimate of β , the fractional change in creep rate due to a fore-
 569 shock, we consider a simple model of periodic locked asperities alternating creeping patches
 570 (Fig. C1). We assume that asperities break in events with uniform stress drop, confined
 571 to a single asperity and the creeping patch on each side, with the next asperity acting
 572 as barrier. Since the response to stress changes is dominated by regions with low σ , we
 573 consider the change in velocity in creeping patches only.

574 The stress field outside a constant stress drop crack of length $2l$ and stress drop
 575 $\Delta\tau$ is (Bonafede et al., 1985):

$$\Delta\tau_{out}(x) = \Delta\tau \frac{|x| - \sqrt{x^2 - l^2}}{\sqrt{x^2 - l^2}} \quad (C6)$$

576 where x is the distance from the crack center on the crack plane. Since the system is sym-
 577 metric around $x = 0$, in what follows we consider $x > 0$. We approximate the stress
 578 change within each creeping patch by the value at its center; as shown in Fig. C1, creep-
 579 ing patches are centered at positions $x = 2l, (2+4/3)l, (2+8/3)l, \dots$. The stress change
 580 at position $x = nl$ is given by

$$\Delta\tau_{out} = \Delta\tau \frac{n - \sqrt{n^2 - 1}}{\sqrt{n^2 - 1}}. \quad (C7)$$

581 The local velocity after a stress step given by the direct effect is

$$V = V_{pre} \exp(\Delta\tau_{out}/a\sigma), \quad (C8)$$

582 where V_{pre} is the velocity before the stress step and σ the normal stress in creeping patches.
 583 Assuming the same initial velocity V_{pre} in all creeping patches, the new average veloc-
 584 ity is the sum of the velocity change in each patch divided by the total number of creep-
 585 ing patches N_p

$$\langle V \rangle = \frac{V_{pre}}{N_p} \sum_{i=0}^{N_p-1} \exp \left[\frac{\Delta\tau}{a\sigma} \left(\frac{n_i - \sqrt{n_i^2 - 1}}{\sqrt{n_i^2 - 1}} \right) \right], \quad (C9)$$

586 where $n_i = 2 + 4i/3$. The fractional change in slip velocity is simply $\beta = \langle V \rangle / V_{pre}$.

587 At the onset of the foreshock sequence considered in the main text, slip velocities in creep-
 588 ing patches are of the order of 10^{-11} m/s (as expected from $V_{cr} \sim \dot{\gamma} / \mu' L_{cr}$), and their
 589 average normal stress is about 5 MPa. Foreshocks have stress drops between 0.1–2 MPa,
 590 with a median value of 0.5 MPa. Considering the nucleation region between 1.7–4.7 km
 591 (Fig. 4), the number of creeping patches is $\approx 3\text{ km} / L_{min} = 30$; and since the analysis
 592 above only considers one side of the fault, $N_p = 15$. Plugging these values into eq. C9
 593 gives β between 1.1 and 1.3, depending on the stress drop.

594 Acknowledgments

595 We would like to thank Aitaro Kato, John Rudnicki and the Associate Editor whose con-
 596 structive reviews helped improve and clarify this manuscript. C.C. was funded by SCEC
 597 award no. 18166 and NSF award no. 1620496. No data was used in this study.

598 **References**

- 599 Abercrombie, R. E., & Mori, J. (1996). Occurrence patterns of foreshocks to large
600 earthquakes in the western United States. *Nature*, *381*(6580), 303–307. (ISBN:
601 0028-0836) doi: 10.1038/381303a0
- 602 Ampuero, J., & Rubin, A. (2008). Earthquake nucleation on rate and state
603 faults Aging and slip laws. *Journal of Geophysical Research: Solid Earth*,
604 *113*(August 2007), 1–61. Retrieved from [http://onlinelibrary.wiley.com/](http://onlinelibrary.wiley.com/doi/10.1029/2007JB005082/full)
605 [doi/10.1029/2007JB005082/full](http://onlinelibrary.wiley.com/doi/10.1029/2007JB005082/full) doi: 10.1029/2007JB005082
- 606 Barcheck, G., Brodsky, E. E., Fulton, P. M., King, M. A., Siegfried, M. R., & Tu-
607 laczyk, S. (2021, February). Migratory earthquake precursors are dominant on
608 an ice stream fault. *Science Advances*, *7*(6), eabd0105. Retrieved 2021-02-21,
609 from <http://advances.sciencemag.org/content/7/6/eabd0105> (Publisher:
610 American Association for the Advancement of Science Section: Research Arti-
611 cle) doi: 10.1126/sciadv.abd0105
- 612 Bonafede, M., Dragoni, M., & Boschi, E. (1985, December). Quasi-static crack
613 models and the frictional stress threshold criterion for slip arrest. *Geo-*
614 *physical Journal International*, *83*(3), 615–635. Retrieved 2020-06-13,
615 from [https://academic.oup.com/gji/article-lookup/doi/10.1111/](https://academic.oup.com/gji/article-lookup/doi/10.1111/j.1365-246X.1985.tb04329.x)
616 [j.1365-246X.1985.tb04329.x](https://academic.oup.com/gji/article-lookup/doi/10.1111/j.1365-246X.1985.tb04329.x) doi: 10.1111/j.1365-246X.1985.tb04329.x
- 617 Bouchon, M., Durand, V., Marsan, D., Karabulut, H., & Schmittbuhl, J. (2013).
618 The long precursory phase of most large interplate earthquakes. *Nature*
619 *Geoscience*, *6*(4), 299–302. Retrieved from [http://dx.doi.org/10.1038/](http://dx.doi.org/10.1038/ngeo1770)
620 [ngeo1770](http://dx.doi.org/10.1038/ngeo1770) (Publisher: Nature Publishing Group) doi: 10.1038/ngeo1770
- 621 Bouchon, M., Karabulut, H., Aktar, M., zalaybey, S., Schmittbuhl, J., & Bouin,
622 M. P. (2011). Extended nucleation of the 1999 Mw 7.6 Izmit earthquake.
623 *Science*, *331*(6019), 877–880. (ISBN: 1095-9203 (Electronic)\r0036-8075 (Link-
624 ing)) doi: 10.1126/science.1197341
- 625 Brodsky, E. E., Kirkpatrick, J. D., & Candela, T. (2016, January). Constraints
626 from fault roughness on the scale-dependent strength of rocks. *Geology*, *44*(1),
627 19–22. Retrieved 2020-04-15, from [http://pubs.geoscienceworld.org/](http://pubs.geoscienceworld.org/geology/article/44/1/19/131963/Constraints-from-fault-roughness-on-the-scale)
628 [geology/article/44/1/19/131963/Constraints-from-fault-roughness-on-](http://pubs.geoscienceworld.org/geology/article/44/1/19/131963/Constraints-from-fault-roughness-on-the-scale)
629 [-the-scale](http://pubs.geoscienceworld.org/geology/article/44/1/19/131963/Constraints-from-fault-roughness-on-the-scale) (Publisher: GeoScienceWorld) doi: 10.1130/G37206.1
- 630 Brodsky, E. E., & van der Elst, N. J. (2014). The Uses of Dynamic Earth-

- 631 quake Triggering. *Annual Review of Earth and Planetary Sciences*, 42(1),
 632 317–339. Retrieved from [http://www.annualreviews.org/doi/10.1146/](http://www.annualreviews.org/doi/10.1146/annurev-earth-060313-054648)
 633 [annurev-earth-060313-054648](http://www.annualreviews.org/doi/10.1146/annurev-earth-060313-054648) doi: 10.1146/annurev-earth-060313-054648
- 634 Candela, T., Renard, F., Bouchon, M., Brouste, A., Marsan, D., Schmittbuhl, J.,
 635 & Voisin, C. (2009). Characterization of fault roughness at various scales:
 636 Implications of three-dimensional high resolution topography measurements.
 637 *Pure and Applied Geophysics*, 166(10-11), 1817–1851. (arXiv: 0810.1109 ISBN:
 638 0033-4553) doi: 10.1007/s00024-009-0521-2
- 639 Candela, T., Renard, F., Klinger, Y., Mair, K., Schmittbuhl, J., &
 640 Brodsky, E. E. (2012). Roughness of fault surfaces over nine
 641 decades of length scales. *Journal of Geophysical Research: Solid*
 642 *Earth*, 117(B8). Retrieved 2020-04-15, from [http://agupubs](http://agupubs.onlinelibrary.wiley.com/doi/abs/10.1029/2011JB009041)
 643 [.onlinelibrary.wiley.com/doi/abs/10.1029/2011JB009041](http://agupubs.onlinelibrary.wiley.com/doi/abs/10.1029/2011JB009041) (_eprint:
 644 <https://onlinelibrary.wiley.com/doi/pdf/10.1029/2011JB009041>) doi:
 645 10.1029/2011JB009041
- 646 Cattania, C., & Segall, P. (2019). Crack models of repeating earthquakes predict
 647 observed moment-recurrence scaling. *Journ. Geophys. Res.*, 124(1), 476–503.
 648 Retrieved 2019-07-17, from [https://agupubs.onlinelibrary.wiley.com/](https://agupubs.onlinelibrary.wiley.com/doi/abs/10.1029/2018JB016056)
 649 [doi/abs/10.1029/2018JB016056](https://agupubs.onlinelibrary.wiley.com/doi/abs/10.1029/2018JB016056) doi: 10.1029/2018JB016056
- 650 Chen, X., & Shearer, P. M. (2013). California foreshock sequences suggest aseismic
 651 triggering process. *Geophys. Res. Lett.*, 40(April), 2602–2607. doi: 10.1002/grl
 652 .50444
- 653 Chester, F. M., & Chester, J. S. (2000, October). Stress and deformation along wavy
 654 frictional faults. *Journal of Geophysical Research: Solid Earth*, 105(B10),
 655 23421–23430. Retrieved 2019-09-27, from [http://agupubs.onlinelibrary](http://agupubs.onlinelibrary.wiley.com/doi/10.1029/2000JB900241)
 656 [.wiley.com/doi/10.1029/2000JB900241](http://agupubs.onlinelibrary.wiley.com/doi/10.1029/2000JB900241) doi: 10.1029/2000JB900241
- 657 Day, S. M., Dalguer, L. A., Lapusta, N., & Liu, Y. (2005). Compar-
 658 ison of finite difference and boundary integral solutions to three-
 659 dimensional spontaneous rupture. *Journal of Geophysical Research:*
 660 *Solid Earth*, 110(B12). Retrieved 2020-05-28, from [http://agupubs](http://agupubs.onlinelibrary.wiley.com/doi/abs/10.1029/2005JB003813)
 661 [.onlinelibrary.wiley.com/doi/abs/10.1029/2005JB003813](http://agupubs.onlinelibrary.wiley.com/doi/abs/10.1029/2005JB003813) (_eprint:
 662 <https://onlinelibrary.wiley.com/doi/pdf/10.1029/2005JB003813>) doi:
 663 10.1029/2005JB003813

- 664 Dieterich, J. H. (1978, July). Time-dependent friction and the mechanics of stick-
 665 slip. *pure and applied geophysics*, *116*(4), 790–806. Retrieved 2020-01-30, from
 666 <https://doi.org/10.1007/BF00876539> doi: 10.1007/BF00876539
- 667 Dieterich, J. H. (1992). Earthquake nucleation on faults with rate-and state-
 668 dependent strength. *Tectonophysics*, *211*(1-4), 115–134. (ISBN: 0040-1951)
 669 doi: 10.1016/0040-1951(92)90055-B
- 670 Dieterich, J. H., & Kilgore, B. (1996, April). Implications of fault constitutive prop-
 671 erties for earthquake prediction. *Proceedings of the National Academy of Sci-*
 672 *ences*, *93*(9), 3787–3794. Retrieved 2019-12-01, from [https://www.pnas.org/](https://www.pnas.org/content/93/9/3787)
 673 [content/93/9/3787](https://www.pnas.org/content/93/9/3787) doi: 10.1073/pnas.93.9.3787
- 674 Dublanchet, P. (2018, February). The dynamics of earthquake precursors controlled
 675 by effective friction. *Geophysical Journal International*, *212*(2), 853–871. Re-
 676 trieved 2019-12-01, from [http://academic.oup.com/gji/article/212/2/](http://academic.oup.com/gji/article/212/2/853/4554385)
 677 [853/4554385](http://academic.oup.com/gji/article/212/2/853/4554385) doi: 10.1093/gji/ggx438
- 678 Dunham, E. M., Belanger, D., Cong, L., & Kozdon, J. E. (2011). Earthquake Rup-
 679 tures with Strongly Rate-Weakening Friction and Off-Fault Plasticity , Part 2:
 680 Nonplanar Faults. *Bulletin of the Seismological Society of America*, *101*(5),
 681 2308–2322. doi: 10.1785/0120100076
- 682 Ellsworth, W. L., & Bulut, F. (2018, July). Nucleation of the 1999 Izmit earth-
 683 quake by a triggered cascade of foreshocks. *Nature Geoscience*, *11*(7), 531–
 684 535. Retrieved 2019-12-19, from [https://www.nature.com/articles/](https://www.nature.com/articles/s41561-018-0145-1)
 685 [s41561-018-0145-1](https://www.nature.com/articles/s41561-018-0145-1) doi: 10.1038/s41561-018-0145-1
- 686 Ende, M., & Ampuero, J. (2020, January). On the statistical significance of
 687 foreshock sequences in Southern California. *Geophysical Research Letters*,
 688 2019GL086224. Retrieved 2020-01-30, from [https://onlinelibrary.wiley](https://onlinelibrary.wiley.com/doi/abs/10.1029/2019GL086224)
 689 [.com/doi/abs/10.1029/2019GL086224](https://onlinelibrary.wiley.com/doi/abs/10.1029/2019GL086224) doi: 10.1029/2019GL086224
- 690 Erickson, B. A., Jiang, J., Barall, M., Lapusta, N., Dunham, E. M., Harris, R.,
 691 ... Wei, M. (2020, March). The community code verification exercise
 692 for simulating sequences of earthquakes and aseismic slip (SEAS). *Seis-*
 693 *mological Research Letters*, *91*(2A), 874–890. Retrieved 2020-05-28, from
 694 <http://pubs.geoscienceworld.org/srl/article/91/2A/874/580609/>
 695 [The-Community-Code-Verification-Exercise-for](http://pubs.geoscienceworld.org/srl/article/91/2A/874/580609/) (Publisher: GeoScience-
 696 World) doi: 10.1785/0220190248

- 697 Fang, Z., & Dunham, E. M. (2013). Additional shear resistance from fault rough-
698 ness and stress levels on geometrically complex faults. *Journal of Geophysical*
699 *Research: Solid Earth*, *118*(7), 3642–3654. (ISBN: 2169-9356) doi: 10.1002/
700 jgrb.50262
- 701 Felzer, K. R., Page, M. T., & Michael, A. J. (2015, February). Artificial seismic
702 acceleration. *Nature Geoscience*, *8*(2), 82–83. Retrieved 2020-11-20, from
703 <http://www.nature.com/articles/ngeo2358> (Number: 2 Publisher: Nature
704 Publishing Group) doi: 10.1038/ngeo2358
- 705 Gomberg, J. (2018, July). Unsettled earthquake nucleation. *Nature Geoscience*,
706 *11*(7), 463–464. Retrieved 2019-12-20, from [https://www.nature.com/](https://www.nature.com/articles/s41561-018-0149-x)
707 [articles/s41561-018-0149-x](https://www.nature.com/articles/s41561-018-0149-x) doi: 10.1038/s41561-018-0149-x
- 708 Hardebeck, J. L., Felzer, K. R., & Michael, A. J. (2008, August). Improved tests
709 reveal that the accelerating moment release hypothesis is statistically insignif-
710 icant: new tests contradict amr hypothesis. *Journal of Geophysical Research:*
711 *Solid Earth*, *113*(B8). Retrieved 2019-12-20, from [http://doi.wiley.com/](http://doi.wiley.com/10.1029/2007JB005410)
712 [10.1029/2007JB005410](http://doi.wiley.com/10.1029/2007JB005410) doi: 10.1029/2007JB005410
- 713 Heimisson, E. R. (2020, May). Crack to pulse transition and magnitude
714 statistics during earthquake cycles on a self-similar rough fault. *Earth*
715 *and Planetary Science Letters*, *537*, 116202. Retrieved 2020-04-17, from
716 <http://www.sciencedirect.com/science/article/pii/S0012821X2030145X>
717 doi: 10.1016/j.epsl.2020.116202
- 718 Helmstetter, A., & Sornette, D. (2003, October). Foreshocks explained by cas-
719 cades of triggered seismicity. *Journal of Geophysical Research: Solid Earth*,
720 *108*(B10). Retrieved 2019-12-20, from [http://doi.wiley.com/10.1029/](http://doi.wiley.com/10.1029/2003JB002409)
721 [2003JB002409](http://doi.wiley.com/10.1029/2003JB002409) doi: 10.1029/2003JB002409
- 722 Jones, L. M., & Molnar, P. (1976). Frequency of foreshocks. *Nature*, *262*.
- 723 Jones, L. M., & Molnar, P. (1979). Some characteristics of foreshocks and their
724 possible relationship to earthquake prediction and premonitory slip on faults.
725 *Journal Geophys. Res.*, *84*(9), 3596–3608.
- 726 Kato, A., Fukuda, J., Kumazawa, T., & Nakagawa, S. (2016, April). Accelerated
727 nucleation of the 2014 Iquique, Chile Mw 8.2 Earthquake. *Scientific Reports*,
728 *6*(1), 24792. Retrieved 2020-11-02, from [http://www.nature.com/articles/](http://www.nature.com/articles/srep24792)
729 [srep24792](http://www.nature.com/articles/srep24792) (Number: 1 Publisher: Nature Publishing Group) doi: 10.1038/

730 srep24792

731 Kato, A., Fukuda, J., Nakagawa, S., & Obara, K. (2016). Foreshock migration pre-
 732 ceding the 2016 Mw 7.0 Kumamoto earthquake, Japan. *Geophysical Research*
 733 *Letters*, *43*(17), 8945–8953. Retrieved 2020-10-28, from [https://agupubs](https://agupubs.onlinelibrary.wiley.com/doi/abs/10.1002/2016GL070079)
 734 [.onlinelibrary.wiley.com/doi/abs/10.1002/2016GL070079](https://agupubs.onlinelibrary.wiley.com/doi/abs/10.1002/2016GL070079) (_eprint:
 735 <https://agupubs.onlinelibrary.wiley.com/doi/pdf/10.1002/2016GL070079>) doi:
 736 10.1002/2016GL070079

737 Kato, A., Obara, K., Igarashi, T., Tsuruoka, H., Nakagawa, S., & Hirata, N. (2012).
 738 Propagation of slow slip leading up to the 2011 Mw9.0 Tohoku-Oki earth-
 739 quake. *Science*, *335*, 705–709. doi: 10.1126/science.1215141

740 Lapusta, N. (2003). Nucleation and early seismic propagation of small and large
 741 events in a crustal earthquake model. *Journal of Geophysical Research*, *108*, 1–
 742 18. (ISBN: 2156-2202) doi: 10.1029/2001JB000793

743 Lapusta, N., Rice, J. R., Ben-Zion, Y., & Zheng, G. (2000, October). Elas-
 744 todynamic analysis for slow tectonic loading with spontaneous rupture
 745 episodes on faults with rate- and state-dependent friction. *Journal of Geo-*
 746 *physical Research: Solid Earth*, *105*(B10). Retrieved 2019-02-15, from
 747 <http://doi.wiley.com/10.1029/2000JB900250> (Publisher: John Wiley
 748 & Sons, Ltd) doi: 10.1029/2000JB900250

749 Lui, S. K. Y., & Lapusta, N. (2016, October). Repeating microearthquake se-
 750 quences interact predominantly through postseismic slip. *Nature Communi-*
 751 *cations*, *7*(1), 13020. Retrieved 2020-11-02, from [http://www.nature.com/](http://www.nature.com/articles/ncomms13020)
 752 [articles/ncomms13020](http://www.nature.com/articles/ncomms13020) (Number: 1 Publisher: Nature Publishing Group)
 753 doi: 10.1038/ncomms13020

754 McGuire, J. J., Boettcher, M., & Jordan, T. H. (2005). Foreshock sequences and
 755 short-term earthquake predictability on east Pacific rise transform faults. *Na-*
 756 *ture*, *434*, 457–461.

757 McLaskey, G. C. (2019, December). Earthquake initiation from labora-
 758 tory observations and implications for foreshocks. *Journal of Geophys-*
 759 *ical Research: Solid Earth*, 2019JB018363. Retrieved 2019-12-20, from
 760 <https://onlinelibrary.wiley.com/doi/abs/10.1029/2019JB018363> doi:
 761 10.1029/2019JB018363

762 McLaskey, G. C., & Lockner, D. A. (2014, August). Preslip and cascade processes

- 763 initiating laboratory stick slip. *Journal of Geophysical Research: Solid Earth*,
 764 119(8), 6323–6336. Retrieved 2019-12-20, from [http://doi.wiley.com/](http://doi.wiley.com/10.1002/2014JB011220)
 765 10.1002/2014JB011220 doi: 10.1002/2014JB011220
- 766 Mignan, A. (2014, January). The debate on the prognostic value of earthquake
 767 foreshocks: a meta-analysis. *Scientific reports*, 4, 4099. Retrieved 2015-01-09,
 768 from [http://www.pubmedcentral.nih.gov/articlerender.fcgi?artid=](http://www.pubmedcentral.nih.gov/articlerender.fcgi?artid=3924212&tool=pmcentrez&rendertype=abstract)
 769 3924212&tool=pmcentrez&rendertype=abstract doi: 10.1038/srep04099
- 770 Noda, H., Nakatani, M., & Hori, T. (2013). Large nucleation before large earth-
 771 quakes is sometimes skipped due to cascade-up Implications from a rate and
 772 state simulation of faults with hierarchical asperities. *Journal of Geophys-*
 773 *ical Research: Solid Earth*, 118(6), 2924–2952. Retrieved 2020-01-29, from
 774 <https://agupubs.onlinelibrary.wiley.com/doi/abs/10.1002/jgrb.50211>
 775 doi: 10.1002/jgrb.50211
- 776 Ogata, Y., Utsu, T., & Katsura, K. (1995, April). Statistical features of fore-
 777 shocks in comparison with other earthquake clusters. *Geophysical Jour-*
 778 *nal International*, 121(1), 233–254. Retrieved 2020-06-17, from [http://](http://academic.oup.com/gji/article/121/1/233/601743)
 779 academic.oup.com/gji/article/121/1/233/601743 (tex.ids: Ogata1995
 780 publisher: Oxford Academic) doi: 10.1111/j.1365-246X.1995.tb03524.x
- 781 Ozawa, S. W., Hatano, T., & Kame, N. (2019). Longer Migration and Sponta-
 782 neous Decay of Aseismic Slip Pulse Caused by Fault Roughness. *Geophys-*
 783 *ical Research Letters*, 46(2), 636–643. Retrieved 2020-10-28, from [http://](http://agupubs.onlinelibrary.wiley.com/doi/abs/10.1029/2018GL081465)
 784 agupubs.onlinelibrary.wiley.com/doi/abs/10.1029/2018GL081465
 785 (_eprint: <https://onlinelibrary.wiley.com/doi/pdf/10.1029/2018GL081465>)
 786 doi: 10.1029/2018GL081465
- 787 Perfettini, H., & Ampuero, J.-P. (2008, September). Dynamics of a velocity
 788 strengthening fault region: Implications for slow earthquakes and postseis-
 789 mic slip. *Journal of Geophysical Research*, 113(B9), B09411. Retrieved
 790 2019-08-09, from <http://doi.wiley.com/10.1029/2007JB005398> doi:
 791 10.1029/2007JB005398
- 792 Persson, B. N. J., Albohr, O., Tartaglino, U., Volokitin, A. I., & Tosatti, E. (2005,
 793 January). On the nature of surface roughness with application to con-
 794 tact mechanics, sealing, rubber friction and adhesion. *Journal of Physics.*
 795 *Condensed Matter: An Institute of Physics Journal*, 17(1), R1–R62. doi:

796 10.1088/0953-8984/17/1/R01

797 Power, W. L., & Tullis, T. E. (1991). Euclidean and fractal models for
 798 the description of rock surface roughness. *Journal of Geophysical Re-*
 799 *search: Solid Earth*, 96(B1), 415–424. Retrieved 2020-04-15, from
 800 <http://agupubs.onlinelibrary.wiley.com/doi/abs/10.1029/90JB02107>
 801 (_eprint: <https://onlinelibrary.wiley.com/doi/pdf/10.1029/90JB02107>) doi:
 802 10.1029/90JB02107

803 Power, W. L., Tullis, T. E., Brown, S. R., Boitnott, G. N., & Scholz, C. H.
 804 (1987). Roughness of natural fault surfaces. *Geophysical Research*
 805 *Letters*, 14(1), 29–32. Retrieved 2020-04-15, from <http://agupubs>
 806 [.onlinelibrary.wiley.com/doi/abs/10.1029/GL014i001p00029](http://agupubs.onlinelibrary.wiley.com/doi/abs/10.1029/GL014i001p00029) (_eprint:
 807 <https://onlinelibrary.wiley.com/doi/pdf/10.1029/GL014i001p00029>) doi:
 808 10.1029/GL014i001p00029

809 Power, W. L., Tullis, T. E., & Weeks, J. D. (1988). Roughness and wear
 810 during brittle faulting. *Journal of Geophysical Research: Solid Earth*,
 811 93(B12), 15268–15278. Retrieved 2020-04-15, from <http://agupubs>
 812 [.onlinelibrary.wiley.com/doi/abs/10.1029/JB093iB12p15268](http://agupubs.onlinelibrary.wiley.com/doi/abs/10.1029/JB093iB12p15268) (_eprint:
 813 <https://onlinelibrary.wiley.com/doi/pdf/10.1029/JB093iB12p15268>) doi:
 814 10.1029/JB093iB12p15268

815 Renard, F., & Candela, T. (2017). Scaling of fault roughness and im-
 816 plications for earthquake mechanics. In *Fault Zone Dynamic Pro-*
 817 *cesses* (pp. 195–215). American Geophysical Union (AGU). Re-
 818 trieved 2020-06-17, from <http://agupubs.onlinelibrary.wiley>
 819 [.com/doi/abs/10.1002/9781119156895.ch10](http://agupubs.onlinelibrary.wiley.com/doi/abs/10.1002/9781119156895.ch10) (Section: 10 _eprint:
 820 <https://onlinelibrary.wiley.com/doi/pdf/10.1002/9781119156895.ch10>) doi:
 821 10.1002/9781119156895.ch10

822 Rice, J. R. (1993). Spatio-temporal complexity of slip on a fault. *Journal of Geo-*
 823 *physical Research*, 98(B6), 9885. (ISBN: 2156-2202) doi: 10.1029/93JB00191

824 Romanet, P., Sato, D., & Ando, R. (2019, November). Curvature, a mechanical link
 825 between the geometrical complexities of a fault. *arXiv:1911.02686 [physics]*.
 826 Retrieved 2020-01-30, from <http://arxiv.org/abs/1911.02686> (arXiv:
 827 1911.02686)

828 Romanet, P., Sato, D. S., & Ando, R. (2020, September). Curvature, a mechani-

- 829 cal link between the geometrical complexities of a fault: application to bends,
 830 kinks and rough faults. *Geophysical Journal International*, 223(1), 211–232.
 831 Retrieved 2020-10-28, from [http://academic.oup.com/gji/article/223/1/](http://academic.oup.com/gji/article/223/1/211/5860282)
 832 211/5860282 (Publisher: Oxford Academic) doi: 10.1093/gji/ggaa308
- 833 Rubin, A. M. (2008, November). Episodic slow slip events and rate-and-state fric-
 834 tion. *Journal of Geophysical Research*, 113(B11), B11414. Retrieved 2019-02-
 835 15, from <http://doi.wiley.com/10.1029/2008JB005642> (Publisher: John
 836 Wiley & Sons, Ltd) doi: 10.1029/2008JB005642
- 837 Rubin, A. M., & Ampuero, J. (2005). Earthquake nucleation on (aging) rate and
 838 state faults. *Journal of Geophysical Research*, 110(2), 1–24. doi: 10.1029/
 839 2005JB003686
- 840 Ruina, A. (1983). Slip instability and state variable friction law. *J. Geophys.*
 841 *Res.*, 88, 10359–10370. Retrieved from [http://onlinelibrary.wiley.com/](http://onlinelibrary.wiley.com/doi/10.1029/JB088iB12p10359/abstract)
 842 doi/10.1029/JB088iB12p10359/abstract (ISBN: 0148-0227) doi: 10.1029/
 843 JB088iB12p10359
- 844 Ruiz, S., Metois, M., Fuenzalida, A., Ruiz, J., Leyton, F., Grandin, R., . . . Campos,
 845 J. (2014). Intense foreshocks and a slow slip event preceded the 2014 Iquique.
 846 *Science*, 345(6201). doi: 10.1126/science.1256074
- 847 Sagy, A., Brodsky, E. E., & Axen, G. J. (2007). Evolution of fault-surface roughness
 848 with slip. *Geology*, 35(3), 283–286. (ISBN: 0091-7613) doi: 10.1130/G23235A
 849 .1
- 850 Sagy, A., & Lyakhovsky, V. (2019). Stress patterns and failure around rough in-
 851 terlocked fault surface. *Journal of Geophysical Research: Solid Earth*, 124(7),
 852 7138–7154. Retrieved 2019-12-18, from [https://agupubs.onlinelibrary](https://agupubs.onlinelibrary.wiley.com/doi/abs/10.1029/2018JB017006)
 853 [.wiley.com/doi/abs/10.1029/2018JB017006](https://agupubs.onlinelibrary.wiley.com/doi/abs/10.1029/2018JB017006) doi: 10.1029/2018JB017006
- 854 Schaal, N., & Lapusta, N. (2019, February). Microseismicity on Patches of Higher
 855 Compression During LargerScale Earthquake Nucleation in a RateandState
 856 Fault Model. *Journal of Geophysical Research: Solid Earth*, 124(2), 1962–
 857 1990. Retrieved 2019-12-20, from [https://onlinelibrary.wiley.com/doi/](https://onlinelibrary.wiley.com/doi/abs/10.1029/2018JB016395)
 858 [abs/10.1029/2018JB016395](https://onlinelibrary.wiley.com/doi/abs/10.1029/2018JB016395) doi: 10.1029/2018JB016395
- 859 Schurr, B., Asch, G., Hainzl, S., Bedford, J., Hoechner, A., Palo, M., . . . Vilotte,
 860 J.-P. (2014). Gradual unlocking of plate boundary controlled initiation of
 861 the 2014 Iquique earthquake. *Nature*, 512(7514), 299–302. Retrieved from

- 862 <http://www.nature.com/doi/10.1038/nature13681> (ISBN: 1476-
863 4687) doi: 10.1038/nature13681
- 864 Segall, P. (2010). *Earthquake and Volcano deformation*. Retrieved from [http://doi](http://doi.wiley.com/10.1002/0471743984.vse7429)
865 [.wiley.com/10.1002/0471743984.vse7429](http://doi.wiley.com/10.1002/0471743984.vse7429) (Princeton University Press) doi:
866 10.1002/0471743984.vse7429
- 867 Segall, P., & Bradley, A. M. (2012). The Role of Thermal Pressurization and
868 Dilatancy in Controlling the Rate of Fault Slip. *J. Applied Mech.*, 79(3),
869 31013. Retrieved from <http://dx.doi.org/10.1115/1.4005896> doi:
870 10.1115/1.4005896
- 871 Sugan, M., Kato, A., Miyake, H., Nakagawa, S., & Vuan, A. (2014). The
872 preparatory phase of the 2009 Mw 6.3 L'Aquila earthquake by improving
873 the detection capability of low-magnitude foreshocks. *Geophysical Re-*
874 *search Letters*, 41(17), 6137–6144. Retrieved 2019-12-01, from [http://](http://agupubs.onlinelibrary.wiley.com/doi/abs/10.1002/2014GL061199)
875 agupubs.onlinelibrary.wiley.com/doi/abs/10.1002/2014GL061199 doi:
876 10.1002/2014GL061199
- 877 Tal, Y., Hager, B. H., & Ampuero, J. P. (2018, January). The Effects of Fault
878 Roughness on the Earthquake Nucleation Process. *Journal of Geophysi-*
879 *cal Research: Solid Earth*, 123(1), 437–456. Retrieved 2019-09-27, from
880 <http://agupubs.onlinelibrary.wiley.com/doi/10.1002/2017JB014746>
881 doi: 10.1002/2017JB014746
- 882 Tape, C., Holtkamp, S., Silwal, V., Hawthorne, J., Kaneko, Y., Ampuero, J. P.,
883 ... West, M. E. (2018, July). Earthquake nucleation and fault slip com-
884 plexity in the lower crust of central Alaska. *Nature Geoscience*, 11(7),
885 536–541. Retrieved 2019-12-20, from [http://www.nature.com/articles/](http://www.nature.com/articles/s41561-018-0144-2)
886 [s41561-018-0144-2](http://www.nature.com/articles/s41561-018-0144-2) doi: 10.1038/s41561-018-0144-2
- 887 Thomas, M. Y., Lapusta, N., Noda, H., & Avouac, J. P. (2014). Quasi-dynamic
888 versus fully dynamic simulations of earthquakes and aseismic slip with and
889 without enhanced coseismic weakening. *Journal of Geophysical Research: Solid*
890 *Earth*, 119(3), 1986–2004. (ISBN: 2169-9313) doi: 10.1002/2013JB010615
- 891 Trugman, D. T., & Ross, Z. E. (2019, August). Pervasive foreshock activity across
892 Southern California. *Geophysical Research Letters*, 46(15), 8772–8781. Re-
893 trieved 2019-12-20, from [https://onlinelibrary.wiley.com/doi/abs/](https://onlinelibrary.wiley.com/doi/abs/10.1029/2019GL083725)
894 [10.1029/2019GL083725](https://onlinelibrary.wiley.com/doi/abs/10.1029/2019GL083725) doi: 10.1029/2019GL083725

895 Yabe, S., & Ide, S. (2018, August). Variations in precursory slip behavior resulting
896 from frictional heterogeneity. *Progress in Earth and Planetary Science*, 5(1),
897 43. Retrieved 2019-12-01, from [https://doi.org/10.1186/s40645-018-0201](https://doi.org/10.1186/s40645-018-0201-x)
898 -x doi: 10.1186/s40645-018-0201-x

899 Yoon, C. E., Yoshimitsu, N., Ellsworth, W. L., & Beroza, G. C. (2019). Foreshocks
900 and mainshock nucleation of the 1999 Mw 7.1 Hector Mine, California, earth-
901 quake. *Journal of Geophysical Research: Solid Earth*, 124(2), 1569–1582.
902 Retrieved 2019-12-01, from [http://agupubs.onlinelibrary.wiley.com/doi/](http://agupubs.onlinelibrary.wiley.com/doi/abs/10.1029/2018JB016383)
903 [abs/10.1029/2018JB016383](http://agupubs.onlinelibrary.wiley.com/doi/abs/10.1029/2018JB016383) doi: 10.1029/2018JB016383